SIAM J. SCI. COMPUT.
Vol. 41, No. 4, pp. B816–B842

A CHARGE-CONSERVATIVE FINITE ELEMENT METHOD FOR INDUCTIONLESS MHD EQUATIONS. PART II: A ROBUST SOLVER*

LINGXIAO LI†, MINGJIU NI‡, AND WEIYING ZHENG§

Abstract. In [L. Li, M. Ni, and W. Zheng, *SIAM J. Sci. Comput.*, 41 (2019), pp. B796–B815] a charge-conservative finite element method is proposed for solving inductionless and incompressible magnetohydrodynamic (MHD) equations. The purpose of this paper is to propose a robust solver for the discrete problem. Using the framework of field-of-values-equivalence, we first study the preconditioned Krylov space method for the continuous problem in the setting of Hilbert spaces. The algebraic preconditioner for the discrete problem is then obtained by representing the preconditioner for the continuous problem in finite element spaces. By three numerical examples, the optimality of the solver to the number of unknowns is demonstrated for both stationary and time-dependent MHD problems.

Key words. inductionless MHD equations, block preconditioner, field-of-values-equivalence, conservation of charges, augmented Lagrangian finite element method

AMS subject classifications. 65M60, 76W05

DOI. 10.1137/19M1260372

1. Introduction.

The incompressible magnetohydrodynamic (MHD) equations describe the dynamic behavior of an electrically conducting fluid under the influence of a magnetic field. They occur in models for fusion reactor blankets, liquid metal magnetic pumps, and aluminum electrolysis, among others (see [1, 25]). In the first part of this study [20], we proposed a charge-conservative finite element method for solving the inductionless MHD model in a dimensionless form,

$$\partial_t \boldsymbol{u} + \boldsymbol{u}\cdot\nabla\boldsymbol{u} - \frac{1}{R_e}\Delta\boldsymbol{u} + \nabla p - \kappa \boldsymbol{J}\times\boldsymbol{B} = \boldsymbol{f} \quad \text{in } \Omega, \tag{1.1a}$$

$$\boldsymbol{J} + \nabla\phi - \boldsymbol{u}\times\boldsymbol{B} = \boldsymbol{0} \quad \text{in } \Omega, \tag{1.1b}$$

$$\operatorname{div}\boldsymbol{u} = 0, \quad \operatorname{div}\boldsymbol{J} = 0 \quad \text{in } \Omega, \tag{1.1c}$$

$$\boldsymbol{u}(0) = \boldsymbol{u}_0 \quad \text{in } \Omega, \tag{1.1d}$$

$$\boldsymbol{u} = \boldsymbol{g} \quad \text{on } \Gamma_{\mathrm{d}}, \tag{1.1e}$$

*Submitted to the journal's Computational Methods in Science and Engineering section July 3, 2018; accepted for publication (in revised form) May 6, 2019; published electronically August 14, 2019.

https://doi.org/10.1137/19M1260372

Funding: The work of the second author was supported in part by China NSF grant 51636009. The work of the third author was supported in part by the National Science Fund for Distinguished Young Scholars 11725106, by China NSF grant 91430215, and by the National Magnetic Confinement Fusion Science Program 2015GB110003.

†Institute of Applied Physics and Computational Mathematics, 100094 Beijing, China (lilingxiao@lsec.cc.ac.cn).

‡School of Engineering Science, University of Chinese Academy of Sciences, 101407 Beijing, China (mjni@ucas.ac.cn).

§NCMIS, LSEC, Institute of Computational Mathematics and Scientific/Engineering Computing, Academy of Mathematics and System Sciences, Chinese Academy of Sciences, 100190 Beijing, China, and School of Mathematical Science, University of Chinese Academy of Sciences, 101407 Beijing, China (zwy@lsec.cc.ac.cn).

$$\frac{1}{R_e}\frac{\partial \boldsymbol{u}}{\partial \boldsymbol{n}} - p\boldsymbol{n} = 0 \quad \text{on } \Gamma_{\mathrm{n}} = \Gamma \backslash \bar{\Gamma}_{\mathrm{d}}, \tag{1.1f}$$

$$\boldsymbol{J} \cdot \boldsymbol{n} = 0 \quad \text{on } \Gamma_{\mathrm{i}}, \tag{1.1g}$$

$$\phi = \xi \quad \text{on } \Gamma_{\mathrm{c}} = \Gamma \backslash \bar{\Gamma}_{\mathrm{i}}, \tag{1.1h}$$

where Ω is a bounded domain with Lipschitz-continuous boundary $\Gamma = \partial\Omega$, $\boldsymbol{n}$ is the unit outer normal to Ω, $\boldsymbol{f}$ is the external force, R_e is the Reynolds number, and κ is the coupling number between the fluid and the electric current density. Let L, t_0, B_0, $u_0 = L/t_0$ be the characteristic quantities of length, time, magnetic induction, and fluid velocity of the system, respectively. The Reynolds number and the coupling number are given by $R_e = \rho L u_0/\nu$ and $\kappa = \sigma L B_0^2/(\rho u_0)$ (see [20]). The initial condition $\boldsymbol{u}_0 \in \boldsymbol{H}^1(\Omega)$ satisfies $\operatorname{div} \boldsymbol{u}_0 = 0$. The unknowns are the velocity $\boldsymbol{u}$, the pressure p, the current density $\boldsymbol{J}$, and the electric scalar potential ϕ. Here $\partial_t \boldsymbol{u}$ denotes the partial derivative of $\boldsymbol{u}$ with respect to t. For inductionless MHD equations, the magnetic induction $\boldsymbol{B}$ can be computed from $\boldsymbol{J}$ by means of the Biot–Savart law. However, since the paper is focused on an efficient preconditioner for solving linearized discrete problems, we assume $\boldsymbol{B}$ is given without loss of generality.

Generally, Γ_{n} denotes the outflow boundary and Γ_{d} denotes the inflow boundary where the velocity is specified. Particularly, the subset $\Gamma_{\mathrm{d}} \cap \{\boldsymbol{g} = 0\}$ stands for fixed wall boundary or no-slip boundary. Here we assume $\Gamma_{\mathrm{d}} \neq \emptyset$ and $\boldsymbol{g} \in \boldsymbol{H}^{1/2}(\Gamma_{\mathrm{d}})$. Since $\operatorname{div} \boldsymbol{u} = 0$, the compatibility of $\boldsymbol{u}$ with the boundary condition requires

$$\boldsymbol{g} \in \left\{ \gamma \boldsymbol{v}|_{\Gamma_{\mathrm{d}}} : \boldsymbol{v} \in \boldsymbol{H}^1(\Omega) \cap \boldsymbol{H}(\operatorname{div} 0, \Omega) \right\},$$

where γ: $\boldsymbol{H}^1(\Omega) \to \boldsymbol{H}^{1/2}(\Gamma)$ denotes the trace operator. Moreover, Γ_{i} denotes insulating boundary and Γ_{c} denotes conductive boundary where $\xi \in H^{1/2}(\Gamma_{\mathrm{c}})$.

The inductionless MHD problem is the coupled system of four unknown functions $(\boldsymbol{u}, p, \boldsymbol{J}, \phi)$. The total number of degrees of freedom (DOFs) could be larger than 10^8 for large Reynolds number or large coupling number on fine meshes. It is very challenging to solve such a large, indefinite, and nonlinear system. The study for efficient and robust preconditioners is an important research area. In 2014, Badia, Martín, and Planas studied a stabilized finite element method for (1.1). They proposed block recursive preconditioners for solving the discrete MHD problem [2]. Their preconditioners are efficient for a relatively high Hartmann number. Since interior penalties are used, the discrete scheme is no longer charge-conservative, namely, $\operatorname{div} \boldsymbol{J}_h \neq 0$.

For fully coupled AMG (algebraic multigrid) and approximate block factorization preconditioners, we refer the reader to the systematic study by Shadid and his collaborators in a series of papers for finite element approximations of various MHD models [7, 33, 34, 35, 36]. Utilizing block factorization of the stiffness matrix and proper approximation of the resulting Schur complement, they developed robust and scalable preconditioners for the Newton–Krylov solver. Numerical experiments show that their solvers also work well for stationary MHD problems (cf., e.g., [36]). In [39], Wathen, Greif, and Schötzau discretized the magnetic field of stationary MHD problems with edge elements and proposed a block preconditioner for solving the linearized discrete problem. Their preconditioner utilizes a combination of effective solvers for the mixed Maxwell and the Navier–Stokes subproblems. They also performed spectral analysis for the "ideal preconditioner," which uses the exact Schur complement. Practically feasible preconditioners are designed by proper simplifications of the Schur complement. Moreover, we refer the reader to [32] for additive Schwarz methods for the time-dependent resistive Hall MHD problem.

Another important class of preconditioners was developed from Krylov space methods in the setting of Hilbert spaces. The main idea is that, once a proper preconditioner is obtained for the continuous problem, and if the discretization of the continuous problem is stable, a robust preconditioner can be designed for the discrete problem by preserving the basic structure of the continuous preconditioner [24]. Two types of preconditioners are developed from this perspective and are called the norm-equivalent preconditioner and the field-of-values- (FOV-) equivalent preconditioner, respectively. The FOV of a matrix $\mathbb{A}$ is defined by $W(\mathbb{A}) := \{\mathbf{v}^*\mathbb{A}\mathbf{v} : \|\mathbf{v}\| = 1\}$. It is a useful tool for proving the convergence of iterative solvers for systems of algebraic equations (see Loghin and Wathen [22]). A right preconditioner $\mathbb{P}$ of $\mathbb{A}$ is said to be FOV-equivalent if $W(\mathbb{A}\mathbb{P})$ is bounded from below and above by two positive constants $C_{\inf}$, $C_{\sup}$, respectively, and the ratio $C_{\inf}/C_{\sup}$ is uniform to sensitive parameters of the problem. In [24], Mardal and Winther extend the norm-equivalence and FOV-equivalence to linear operators on Hilbert spaces. They propose an abstract framework of preconditioned Krylov space methods. Following this framework, Ma et al. proposed norm-equivalent and FOV-equivalent preconditioners for structure-preserving finite element discretization of the full MHD problem [23]. They also proved the robustness of preconditioners with respect to both physical parameters and DOFs. The preconditioner for solving continuous problems can also be found in the paper of Hiptmair [16], where it is called "operator preconditioning."

In this paper, we follow the framework of FOV-equivalence in [22, 23, 24] to propose a preconditioner for solving the charge-conservative finite element problem. We first propose a right preconditioner $\hat{\mathcal{A}}^{-1}$ for solving the linearized continuous problem by virtue of LU factorization of the operator matrix $\mathcal{A}$ of the MHD problem. Using the framework of FOV-equivalence, we prove the convergence rate of the GMRES method for solving the preconditioned problem $(\mathcal{A}\hat{\mathcal{A}}^{-1})\zeta = \chi$. Moreover, we introduce a practically feasible preconditioner $\mathcal{P}$ by simplifying $\hat{\mathcal{A}}$, and we prove the convergence rate of GMRES method for solving $(\hat{\mathcal{A}}\mathcal{P})\ell = \zeta$ under properly defined Hilbert norms. Based on these observations, we propose to precondition the original differential operator $\mathcal{A}$ directly by $\mathcal{P}$. In the discrete setting, let $\mathbb{A}$ and $\mathbb{P}$ be, respectively, the Galerkin matrices of operators $\mathcal{A}$ and $\mathcal{P}$. The preconditioner of $\mathbb{A}$ is therefore chosen as $\mathbb{P}$. Here we would like to specify as follows the differences between this paper and the most relevant references [2, 23, 39]:

- In [2], the authors studied the preconditioners for solving the discrete problem of the stabilized finite element method, while in this paper we study a charge-conservative mixed finite element method.
- In [23], the authors proposed norm-equivalent and FOV-equivalent preconditioners for solving the full MHD model. The linearized flow equations are of Stokes type, and the matrix of differential operators is self-adjoint and positive. In this paper, the linearized flow equations contain the convection term and are of Navier–Stokes type.
- In [39], the authors proposed a block preconditioner for solving the full MHD problem and performed spectral analysis for the *ideal preconditioner with exact Schur complement*. In this paper, we proposed a preconditioner for solving the inductionless MHD model which uses $\boldsymbol{J}$ as an unknown instead of $\boldsymbol{B}$. Moreover, the approximation between the ideal preconditioner and the *practical preconditioner with simplified Schur complement* is also studied within the framework of FOV-equivalence.
- We use augmented Lagrangian stabilization in the weak formulation. This helps us in analyzing the approximation between the ideal preconditioner and the practical preconditioner.

We remark that finite element methods for the full MHD model are naturally charge-conservative, since the discrete magnetic induction $\boldsymbol{B}_h$ is a primitive variable, and the discrete current density is given by $\boldsymbol{J}_h = \mathbf{curl}\, \boldsymbol{B}_h$ (cf. [23, 38, 39] and the references therein). The inductionless MHD model is also widely studied in the literature (cf. [2, 11, 27, 28]). Since $\boldsymbol{J}_h$ is a primitive variable in this model, a finite element method should be properly designed to ensure the conservation of charges.

The paper is organized as follows. In section 2, we present the mixed finite element method for time-dependent MHD equations by using augmented Lagrangian stabilization. The discrete problem is linearized with extrapolated solutions from previous time steps. In section 3, we study a preconditioned GMRES method for solving the continuous MHD problem in the setting of Hilbert spaces. The convergence rate is also proved by using the framework of FOV-equivalence. In section 4, we design the algebraic preconditioner by representing the continuous preconditioner in finite element spaces while keeping its block structure. In section 5, we present three numerical examples for both stationary and time-dependent problems to demonstrate the competitive performance of the solver. In section 6, we conclude the main result of the paper. To keep the paper focused on designing a robust preconditioner, we postpone all proofs to the appendices. Throughout the paper, let vector-valued quantities be denoted by boldface notation, such as $\boldsymbol{L}^2(\Omega) := (L^2(\Omega))^3$, and let $\langle \cdot, \cdot \rangle$ denote the generic duality between a Sobolev space and its dual space.

2. A charge-conservative finite element method. First, we introduce some Sobolev spaces. Let $L^2(\Omega)$ be the space of square-integrable functions with the inner product and norm

$$(u, v) := \int_\Omega uv, \qquad \|u\|_{L^2(\Omega)} := (u, u)^{1/2}.$$

Let $H^1(\Omega)$ ($\boldsymbol{H}(\mathrm{div}, \Omega)$) denote the subspaces of $L^2(\Omega)$ (resp., $\boldsymbol{L}^2(\Omega)$) whose functions have square-integrable gradients (resp., divergences). Let $H^1_0(\Omega)$, $\boldsymbol{H}_0(\mathrm{div}, \Omega)$ denote their subspaces which have, respectively, vanishing traces and vanishing normal traces on $\Gamma := \partial\Omega$. We refer the reader to [13, p. 26] for their definitions and inner products. The subspaces of divergence-free functions are denoted by

$$\boldsymbol{H}(\mathrm{div}\, 0, \Omega) := \{\boldsymbol{v} \in \boldsymbol{H}(\mathrm{div}, \Omega) \,:\, \mathrm{div}\, \boldsymbol{v} = 0\},$$
$$\boldsymbol{H}_0(\mathrm{div}\, 0, \Omega) := \boldsymbol{H}(\mathrm{div}\, 0, \Omega) \cap \boldsymbol{H}_0(\mathrm{div}, \Omega).$$

2.1. Semidiscrete weak formulation. We follow [20] to introduce the finite element approximation of (1.1). For convenience, let the function spaces be denoted, for velocity, by

$$\boldsymbol{V} = \boldsymbol{H}^1(\Omega), \qquad \boldsymbol{V}_{\mathrm{d}} = \{\boldsymbol{v} \in \boldsymbol{V} : \boldsymbol{v} = 0 \ \text{ on } \Gamma_{\mathrm{d}}\},$$

for pressure, by

$$Q = L^2(\Omega) \quad \text{if } \Gamma_{\mathrm{n}} \neq \emptyset; \qquad Q = L^2_0(\Omega) \quad \text{if } \Gamma_{\mathrm{n}} = \emptyset,$$

for current density, by

$$\boldsymbol{D} = \boldsymbol{H}(\mathrm{div}, \Omega), \qquad \boldsymbol{D}_{\mathrm{i}} = \{\boldsymbol{v} \in \boldsymbol{D} : \boldsymbol{v} \cdot \boldsymbol{n} = 0 \ \text{ on } \Gamma_{\mathrm{i}}\},$$

and for electric scalar potential, by

$$S = L^2(\Omega) \quad \text{if } \Gamma_{\mathrm{c}} \neq \emptyset; \qquad S = L^2_0(\Omega) \quad \text{if } \Gamma_{\mathrm{c}} = \emptyset.$$

Let $\{t_n = n\tau : \ n = 0, 1, \ldots, N\}$, $\tau = T/N$, be an equidistant partition of $[0, T]$. For a sequence $\{\boldsymbol{u}_n\}$, define the finite difference, the mean value, and the extrapolation of $\boldsymbol{u}_n$ by

$$\delta_t \boldsymbol{u}_n := \frac{1}{\tau}\left(\boldsymbol{u}_n - \boldsymbol{u}_{n-1}\right), \qquad \bar{\boldsymbol{u}}_n := \frac{1}{2}\left(\boldsymbol{u}_n + \boldsymbol{u}_{n-1}\right), \qquad \boldsymbol{u}_n^* := \frac{1}{2}\left(3\boldsymbol{u}_{n-1} - \boldsymbol{u}_{n-2}\right).$$

Moreover, $\boldsymbol{u}_n^* := \boldsymbol{u}_n$ for $n = 1$. The time averages of given functions are defined by

$$\boldsymbol{g}_n = \frac{1}{\tau}\int_{t_{n-1/2}}^{t_{n+1/2}} \boldsymbol{g}(t)\mathrm{d}t, \qquad \Psi_n = \frac{1}{\tau}\int_{t_{n-1}}^{t_n} \Psi(t)\mathrm{d}t, \quad \Psi = \boldsymbol{B},\ \boldsymbol{f},\ \xi. \tag{2.1}$$

From the analysis in [20], Ψ_n and $\boldsymbol{g}_n$ are second-order approximations to $\Psi(t_{n-1/2})$ and $\boldsymbol{g}(t_n)$, respectively, if they are C^2-smooth in time.

A semidiscrete weak formulation of (1.1) reads as follows: Find $(\boldsymbol{u}_n, p_n, \boldsymbol{J}_n, \phi_n) \in \boldsymbol{V} \times Q \times \boldsymbol{D}_{\mathrm{i}} \times S$, $n > 0$, such that $\gamma \boldsymbol{u}_n = \boldsymbol{g}_n$ on Γ_{d} and

(2.2a)
$$(\delta_t \boldsymbol{u}_n, \boldsymbol{v}) + \mathscr{O}(\boldsymbol{u}_n^*; \bar{\boldsymbol{u}}_n, \boldsymbol{v}) + \mathscr{A}_{\mathrm{AL}}(\bar{\boldsymbol{u}}_n, \boldsymbol{v}) - (p_n, \operatorname{div} \boldsymbol{v}) = (\boldsymbol{f}_n + \kappa \boldsymbol{J}_n \times \boldsymbol{B}_n, \boldsymbol{v}) \quad \forall\, \boldsymbol{v} \in \boldsymbol{V}_{\mathrm{d}},$$

(2.2b)
$$(\boldsymbol{J}_n, \boldsymbol{d}) - (\phi_n, \operatorname{div} \boldsymbol{d}) + (\boldsymbol{B}_n \times \bar{\boldsymbol{u}}_n, \boldsymbol{d}) = \langle \gamma_{\boldsymbol{n}} \boldsymbol{d}, \xi_n \rangle_{\Gamma_{\mathrm{c}}} \quad \forall\, \boldsymbol{d} \in \boldsymbol{D}_{\mathrm{i}},$$

(2.2c)
$$(q, \operatorname{div} \bar{\boldsymbol{u}}_n) = 0 \quad \forall\, q \in Q,$$

(2.2d)
$$(\varphi, \operatorname{div} \boldsymbol{J}_n) = 0 \quad \forall\, \varphi \in S,$$

where the bilinear form $\mathscr{A}_{\mathrm{AL}}$ and the trilinear form $\mathscr{O}$ are defined as follows:

$$\mathscr{A}_{\mathrm{AL}}(\boldsymbol{w}, \boldsymbol{v}) := \frac{1}{R_e}(\nabla \boldsymbol{w}, \nabla \boldsymbol{v}) + \alpha(\operatorname{div} \boldsymbol{w}, \operatorname{div} \boldsymbol{v}),$$
$$\mathscr{O}(\boldsymbol{w}; \boldsymbol{u}, \boldsymbol{v}) := \frac{1}{2}\left[(\boldsymbol{w} \cdot \nabla \boldsymbol{u}, \boldsymbol{v}) - (\boldsymbol{w} \cdot \nabla \boldsymbol{v}, \boldsymbol{u}) + \int_{\Gamma_{\mathrm{n}}} (\gamma_{\boldsymbol{n}}^{\downarrow} \boldsymbol{w})(\boldsymbol{u} \cdot \boldsymbol{v})\right].$$

In $\mathscr{A}_{\mathrm{AL}}$, the term $\alpha(\operatorname{div} \boldsymbol{w}, \operatorname{div} \boldsymbol{v})$ stands for augmented Lagrangian (AL) stabilization, and $\alpha > 0$ is the AL-stabilization parameter. Since the exact solution satisfies $\operatorname{div} \boldsymbol{u} = 0$, it is easy to see that

$$\mathscr{A}_{\mathrm{AL}}(\boldsymbol{u}, \boldsymbol{v}) = \frac{1}{R_e}(\nabla \boldsymbol{u}, \nabla \boldsymbol{v}) \quad \forall\, \boldsymbol{v} \in \boldsymbol{V}_{\mathrm{d}}.$$

Moreover, $\gamma_{\boldsymbol{n}}^{\downarrow} \boldsymbol{w} := \max(\boldsymbol{w} \cdot \boldsymbol{n}, 0)$ stands for the outflow flux on the fixed boundary Γ_{n}.

2.2. Fully discrete finite element scheme. Let $\mathcal{T}_h$ be a quasi-uniform and shape-regular tetrahedral mesh of Ω with mesh size $h = \max_{K \in \mathcal{T}_h} h_K$. For any integer $k \geq 0$, let $P_k(K)$ be the space of polynomials of degree k, and define $\boldsymbol{P}_k(K) = P_k(K)^3$. The finite element subspaces are defined, respectively, as follows:

$$\boldsymbol{V}^h := \{\boldsymbol{v} \in \boldsymbol{V} : \ \boldsymbol{v}|_K \in \boldsymbol{P}_2(K) \ \ \forall\, K \in \mathcal{T}_h\},$$
$$Q^h := \{q \in Q : \ q|_K \in P_1(K) \ \ \forall\, K \in \mathcal{T}_h\} \cap H^1(\Omega),$$
$$\boldsymbol{D}^h := \{\boldsymbol{d} \in \boldsymbol{D} : \ \boldsymbol{d}|_K \in \boldsymbol{P}_1(K) \ \forall\, K \in \mathcal{T}_h\},$$
$$S^h := \{s \in S : \ s|_K \in P_0(K) \ \ \forall\, K \in \mathcal{T}_h\}.$$

The subspaces with homogeneous boundary conditions on $\Gamma_{\rm d}$ or $\Gamma_{\rm i}$ are denoted by

$$\boldsymbol{V}_{\rm d}^h = \boldsymbol{V}_{\rm d} \cap \boldsymbol{V}^h, \qquad \boldsymbol{D}_{\rm i}^h = \boldsymbol{D}_{\rm i} \cap \boldsymbol{D}^h.$$

Let $\boldsymbol{u}_0^h \in \boldsymbol{V}^h$, $\boldsymbol{g}_n^h \in \gamma \boldsymbol{V}^h$ be finite element approximations of $\boldsymbol{u}_0$ and $\boldsymbol{g}_n$ respectively. Following [20], we propose an extrapolated finite element approximation to (2.2) as follows: Find $(\boldsymbol{u}_n^h, p_n^h, \boldsymbol{J}_n^h, \phi_n^h) \in \boldsymbol{V}^h \times Q^h \times \boldsymbol{D}_{\rm i}^h \times S^h$ such that $\gamma \boldsymbol{u}_n^h = \boldsymbol{g}_n^h$ on $\Gamma_{\rm d}$ and

(2.3a)
$$(\delta_t \boldsymbol{u}_n^h, \boldsymbol{v}) + \mathscr{O}(\boldsymbol{u}_n^{h,*}; \bar{\boldsymbol{u}}_n^h, \boldsymbol{v}) + \mathscr{A}_{\rm AL}(\bar{\boldsymbol{u}}_n^h, \boldsymbol{v}) - (p_n^h, \operatorname{div} \boldsymbol{v}) = (\boldsymbol{f}_n + \kappa \boldsymbol{J}_n^h \times \boldsymbol{B}_n, \boldsymbol{v}) \quad \forall\, \boldsymbol{v} \in \boldsymbol{V}_{\rm d}^h,$$

(2.3b)
$$(\boldsymbol{J}_n^h, \boldsymbol{d}) - (\phi_n^h, \operatorname{div} \boldsymbol{d}) + (\boldsymbol{B}_n \times \bar{\boldsymbol{u}}_n^h, \boldsymbol{d}) = \langle \gamma_{\boldsymbol{n}} \boldsymbol{d}, \xi_n^h \rangle_{\Gamma_{\rm c}} \quad \forall\, \boldsymbol{d} \in \boldsymbol{D}_{\rm i}^h,$$

(2.3c)
$$(q, \operatorname{div} \bar{\boldsymbol{u}}_n^h) = 0 \quad \forall\, q \in Q^h,$$

(2.3d)
$$(\varphi, \operatorname{div} \boldsymbol{J}_n^h) = 0 \quad \forall\, \varphi \in S^h,$$

where $\bar{\boldsymbol{u}}_n^h := (\boldsymbol{u}_n^h + \boldsymbol{u}_{n-1}^h)/2$ and $\boldsymbol{u}_n^{h,*} := (3\boldsymbol{u}_{n-1}^h - \boldsymbol{u}_{n-2}^h)/2$. We use $\boldsymbol{u}_1^{h,*} = \boldsymbol{u}_1^h$ for $n = 1$ in (2.3a) and solve a nonlinear problem. For $n > 1$, a linear system of equations results from this approximation.

3. Preconditioned Krylov space method for the linearized semidiscrete problem. Now we are in the position to study the preconditioner for solving the discrete problem (2.3). As remarked previously, finite element methods for the full resistive MHD model are naturally charge-conservative since $\boldsymbol{J}_h = \mathbf{curl}\, \boldsymbol{B}_h$ is divergence-free. Here we mention two classes of efficient preconditioners for finite element discretizations of the full MHD model. The first class is based on the coupling of AMG and approximate block factorizations (cf. [7, 33, 34, 39]). The second class is based on Krylov space methods for solving continuous problems in Hilbert spaces. With this perspective, Mardal and Winther present a framework of norm-equivalent and FOV-equivalent preconditioners for solving systems of partial differential equations in [24]. Following this framework, Ma et al. developed robust norm-equivalent and FOV-equivalent preconditioners for the full MHD model [23].

We are going to follow [22, 23, 24] to study an FOV-equivalent preconditioner for solving (2.3). We also use ideas from block factorizations [7, 33, 34, 39]. The starting point is to study the linearized semidiscrete problem (2.2) in the setting of Hilbert spaces. For simplicity, we only consider $\Gamma_{\rm d} = \Gamma_{\rm i} = \Gamma$. This yields

$$\boldsymbol{V}_{\rm d} = \boldsymbol{V}_0 := \boldsymbol{H}_0^1(\Omega), \qquad \boldsymbol{D}_{\rm i} = \boldsymbol{D}_0 := \boldsymbol{H}_0(\operatorname{div}, \Omega), \qquad Q = S = L_0^2(\Omega).$$

Let $\mathcal{I}_u$, $\mathcal{I}_p$, $\mathcal{I}_J$, $\mathcal{I}_\phi$ be the identity operators on $\boldsymbol{V}$, Q, $\boldsymbol{D}$, and S, respectively. To prove the robustness of preconditioners, we assume throughout this section that

$$\boldsymbol{u}_n^* \in \boldsymbol{V}_0 \cap \boldsymbol{H}(\operatorname{div} 0) \cap \boldsymbol{L}^\infty(\Omega), \qquad \boldsymbol{B}_n \in \boldsymbol{L}^\infty(\Omega).$$

3.1. Operator equation. First, we rewrite (2.2) as an operator equation. Define the linearized convection-diffusion operator $\mathcal{F}_u$: $\boldsymbol{V} \to \boldsymbol{V}_0'$ as follows:

$$\langle \mathcal{F}_u(\boldsymbol{v}), \boldsymbol{w} \rangle = 2\tau^{-1}(\boldsymbol{v}, \boldsymbol{w}) + \mathscr{O}(\boldsymbol{u}_n^*; \boldsymbol{v}, \boldsymbol{w}) + \mathscr{A}_{\rm AL}(\boldsymbol{v}, \boldsymbol{w}) \quad \forall\, \boldsymbol{v} \in \boldsymbol{V},\ \boldsymbol{w} \in \boldsymbol{V}_0.$$

By integration by parts, it can be represented by an explicit form,

$$\mathcal{F}_u := 2\tau^{-1}\mathcal{I}_u + \boldsymbol{u}_n^* \cdot \nabla - R_e^{-1}\Delta - \alpha\nabla\,\mathrm{div}\,. \tag{3.1}$$

Moreover, let $\mathcal{K}$: $\boldsymbol{V} \to \boldsymbol{D}_0'$ be the multiplying operator which satisfies

$$\mathcal{K}(\boldsymbol{v}) = \boldsymbol{B}_n \times \boldsymbol{v} \quad \forall\, \boldsymbol{v} \in \boldsymbol{V}. \tag{3.2}$$

Let $\boldsymbol{w_n} \in \boldsymbol{V}$ be the lifting of the boundary condition $\boldsymbol{g}_n$ such that $\gamma \boldsymbol{w}_n = \boldsymbol{g}_n$ on Γ, and define $\hat{\boldsymbol{u}}_n = \bar{\boldsymbol{u}}_n - \boldsymbol{w}_n \in \boldsymbol{V}_0$. Using (3.1)–(3.2), we can write (2.2) as an equivalent operator form,

$$\begin{pmatrix} \kappa\mathcal{I}_J & \kappa\nabla & \kappa\mathcal{K} & 0 \\ -\kappa\,\mathrm{div} & 0 & 0 & 0 \\ -\kappa\mathcal{K}^* & 0 & \mathcal{F}_u & \nabla \\ 0 & 0 & -\,\mathrm{div} & 0 \end{pmatrix} \begin{pmatrix} \boldsymbol{J}_n \\ \phi_n \\ \hat{\boldsymbol{u}}_n \\ p_n \end{pmatrix} = \begin{pmatrix} 0 \\ 0 \\ f_u \\ 0 \end{pmatrix}, \tag{3.3}$$

where $\mathcal{K}^*$ is the dual operator of $\mathcal{K}$, and $f_u \in \boldsymbol{V}_0'$ is defined by

$$\langle f_u, \boldsymbol{v}\rangle = \big(\boldsymbol{f}_n + 2\tau^{-1}\boldsymbol{u}_{n-1}, \boldsymbol{v}\big) + \langle \mathcal{F}_u \boldsymbol{w}_n, \boldsymbol{v}\rangle \quad \forall\, \boldsymbol{v} \in \boldsymbol{V}_0.$$

Write $\boldsymbol{X} = \boldsymbol{D}_0 \times S \times \boldsymbol{V}_0 \times Q$. The coefficient matrix of (3.3) provides a linear operator

$$\mathcal{A} = \begin{pmatrix} \kappa\mathcal{I}_J & \kappa\nabla & \kappa\mathcal{K} & 0 \\ -\kappa\,\mathrm{div} & 0 & 0 & 0 \\ -\kappa\mathcal{K}^* & 0 & \mathcal{F}_u & \nabla \\ 0 & 0 & -\,\mathrm{div} & 0 \end{pmatrix} : \ \boldsymbol{X} \ \to \ \boldsymbol{X}'.$$

3.2. Block preconditioners based on LU factorization. For convenience, we introduce some notation for linear operators. Define $\mathcal{D}_J := \mathcal{I}_J - \nabla\,\mathrm{div}$. It is easy to see that $\mathcal{D}_J$: $\boldsymbol{D}_0 \to \boldsymbol{D}_0'$ is a self-adjoint, continuous, and positive operator. For any $\boldsymbol{v}, \boldsymbol{w} \in \boldsymbol{H}_0(\mathrm{div}, \Omega)$,

$$\langle \mathcal{D}_J \boldsymbol{v}, \boldsymbol{w}\rangle = (\boldsymbol{v}, \boldsymbol{w}) + (\mathrm{div}\,\boldsymbol{v}, \mathrm{div}\,\boldsymbol{w})$$

provides a coercive bilinear form on $\boldsymbol{H}_0(\mathrm{div}, \Omega)$. The Lax–Milgram lemma shows that $\mathcal{D}_J^{-1}$: $\boldsymbol{D}_0' \to \boldsymbol{D}_0$ exists and is a bounded operator. Define

$$\begin{aligned} &\hat{\mathcal{I}}_\phi = -\,\mathrm{div}\,\mathcal{D}_J^{-1}\nabla, && \hat{\mathcal{I}}_J = \mathcal{D}_J^{-1} + (\mathcal{D}_J^{-1}\nabla)\hat{\mathcal{I}}_\phi^{-1}(\mathrm{div}\,\mathcal{D}_J^{-1}), \\ &\mathcal{F}_\kappa = \mathcal{F}_u + \kappa\mathcal{K}^*\hat{\mathcal{I}}_J\mathcal{K}, && \mathcal{F}_1 := 2\tau^{-1}\mathcal{I}_u - R_e^{-1}\Delta - \alpha\nabla\,\mathrm{div} + \kappa\mathcal{K}^*\hat{\mathcal{I}}_J\mathcal{K}. \end{aligned} \tag{3.4}$$

Clearly $\hat{\mathcal{I}}_\phi$: $S \to S$, $\hat{\mathcal{I}}_J$: $\boldsymbol{D}_0' \to \boldsymbol{D}_0$, and $\mathcal{F}_\kappa$, $\mathcal{F}_1$: $\boldsymbol{V}_0 \to \boldsymbol{V}_0'$ are linear mappings. Moreover, we define

$$\mathcal{L}_p := \alpha_1\mathcal{I}_p - 2\tau^{-1}\Delta_p^{-1}, \qquad \alpha_1 := \alpha + R_e^{-1}, \tag{3.5}$$

where Δ_p: $H^1(\Omega)/\mathbb{R} \to (H^1(\Omega)/\mathbb{R})'$ is the pressure Laplacian operator satisfying

$$\langle \Delta_p \xi, \eta\rangle = -(\nabla\xi, \nabla\eta) \quad \forall\, \xi, \eta \in H^1(\Omega)/\mathbb{R}.$$

By the Friedrichs inequality, Δ_p is continuous and invertible.

Now we consider the factorizations of $\mathcal{A}$. It is easy to see $\mathcal{A} = \mathcal{E}_1\mathcal{A}_1$, where

$$\mathcal{E}_1 = \begin{pmatrix} \mathcal{I}_J & -\nabla & 0 & 0 \\ 0 & \mathcal{I}_\phi & 0 & 0 \\ 0 & 0 & \mathcal{I}_u & 0 \\ 0 & 0 & 0 & \mathcal{I}_p \end{pmatrix}, \qquad \mathcal{A}_1 = \begin{pmatrix} \kappa\mathcal{D}_J & \kappa\nabla & \kappa\mathcal{K} & 0 \\ -\kappa\,\mathrm{div} & 0 & 0 & 0 \\ -\kappa\mathcal{K}^* & 0 & \mathcal{F}_u & \nabla \\ 0 & 0 & -\,\mathrm{div} & 0 \end{pmatrix}.$$

With the notation in (3.4) and (3.5), $\mathcal{A}_1$ can be further factorized into $\mathcal{A}_1 = \mathcal{E}_2\mathcal{A}_2$, where

$$\mathcal{A}_2 = \begin{pmatrix} \kappa\mathcal{D}_J & \kappa\nabla & \kappa\mathcal{K} & 0 \\ 0 & -\kappa\hat{\mathcal{I}}_\phi & \kappa\,\mathrm{div}\,\mathcal{D}_J^{-1}\mathcal{K} & 0 \\ 0 & 0 & \mathcal{F}_\kappa & \nabla \\ 0 & 0 & 0 & \mathrm{div}\,\mathcal{F}_\kappa^{-1}\nabla \end{pmatrix},$$

$$\mathcal{E}_2 = \begin{pmatrix} \mathcal{I}_J & 0 & 0 & 0 \\ -\,\mathrm{div}\,\mathcal{D}_J^{-1} & \mathcal{I}_\phi & 0 & 0 \\ -\mathcal{K}^*\mathcal{D}_J^{-1} & -\mathcal{K}^*\mathcal{D}_J^{-1}\nabla\hat{\mathcal{I}}_\phi^{-1} & \mathcal{I}_u & 0 \\ 0 & 0 & -\,\mathrm{div}\,\mathcal{F}_\kappa^{-1} & \mathcal{I}_p \end{pmatrix}.$$

This shows $\mathcal{A}\hat{\mathcal{A}}^{-1} = \mathcal{E}_1\mathcal{E}_2\mathcal{E}_1^{-1}$, where

$$\hat{\mathcal{A}} := \mathcal{E}_1\mathcal{A}_2 = \begin{pmatrix} \kappa\mathcal{D}_J & \kappa\nabla(\mathcal{I}_\phi + \hat{\mathcal{I}}_\phi) & (2\mathcal{I}_J - \mathcal{D}_J^{-1})\kappa\mathcal{K} & 0 \\ 0 & -\kappa\hat{\mathcal{I}}_\phi & \kappa\,\mathrm{div}\,\mathcal{D}_J^{-1}\mathcal{K} & 0 \\ 0 & 0 & \mathcal{F}_\kappa & \nabla \\ 0 & 0 & 0 & \mathrm{div}\,\mathcal{F}_\kappa^{-1}\nabla \end{pmatrix}. \tag{3.6}$$

Since $\mathcal{E}_1\mathcal{E}_2\mathcal{E}_1^{-1}$ only has unit eigenvalues, this inspires us to use $\hat{\mathcal{A}}$ as a right preconditioner of $\mathcal{A}$.

Since $\hat{\mathcal{A}}$ is complicated, we need to approximate its entries by simple operators. Let $C_p \geq 1$ be the Poincaré constant which satisfies, for all $2 \leq r \leq 6$ and all $v \in H^1(\Omega)/\mathbb{R}$,

$$\|v\|_{L^r(\Omega)} \leq C_p|v|_{H^1(\Omega)}. \tag{3.7}$$

By Lemma A.1, $\hat{\mathcal{I}}_\phi$ is self-adjoint and positive on S and satisfies

$$\left(1 + C_p^2\right)^{-1}(\xi,\xi) \leq \left(\hat{\mathcal{I}}_\phi\xi,\xi\right) \leq (\xi,\xi) \quad \forall\,\xi \in S.$$

From [24], $\hat{\mathcal{I}}_\phi$ is spectrally equivalent to the identity operator $\mathcal{I}_\phi$ on S. This inspires us to approximate $\hat{\mathcal{I}}_\phi$ by $\mathcal{I}_\phi$. Furthermore, the commutator argument implies that $\mathrm{div}\,\mathcal{F}_\kappa^{-1}\nabla$ can be approximated by $-\mathcal{L}_p^{-1}$ (cf., e.g., [9, 14]). The theoretical justification for this approximation is given in Lemma A.4 for the case when the stabilization parameter α is large enough and the time step size τ is small enough.

Now for solving the semidiscrete problem (2.2), we choose the preconditioner of $\hat{\mathcal{A}}$ as follows:

$$\mathcal{P} = \begin{pmatrix} \kappa\mathcal{D}_J & 2\kappa\nabla & 2\kappa\mathcal{K} & 0 \\ 0 & -\kappa\mathcal{I}_\phi & 0 & 0 \\ 0 & 0 & \mathcal{F}_\kappa & \nabla \\ 0 & 0 & 0 & -\mathcal{L}_p^{-1} \end{pmatrix}^{-1}. \tag{3.8}$$

It suffices to study the GMRES method for solving the operator equation, for given $\chi \in \boldsymbol{X}'$,

$$(\mathcal{A}\mathcal{P})\ell = \chi\,. \tag{3.9}$$

Actually, (3.9) can be written equivalently as the system of equations

$$(\mathcal{A}\hat{\mathcal{A}}^{-1})\zeta = \chi\,, \qquad (\hat{\mathcal{A}}\mathcal{P})\ell = \zeta\,. \tag{3.10}$$

It is difficult to prove the convergence rate of the GMRES method for solving (3.9). Instead, we are going to study the convergence rates of GMRES methods for solving both equations in (3.10).

Remark 3.1. By Lemma A.2, the operator $\kappa\mathcal{K}^*\hat{\mathcal{I}}_J\mathcal{K}$ appearing in $\mathcal{F}_\kappa$ is self-adjoint and positive. It describes the braking of an external magnetic field for the conducting fluid. A similar term, $\beta\mathcal{K}^*\mathcal{K}$ for some $\beta > 0$, also appears in preconditioners for the full resistive MHD model (cf., e.g., [21, 39]). Therefore, the inductionless MHD model represents the essential coupling of the magnetic field to the force in the fluid. However, the analysis for the inductionless MHD model is easier than that for the full MHD model since the external field $\boldsymbol{B}$ can be a regular function.

3.3. Convergence rates of GMRES methods for solving (3.10). We use the abstract framework of FOV-equivalence to prove the convergence rates of GMRES methods for solving (3.10) (see [22, 23, 24]). For any Hilbert space X, let $\mathcal{L}$: $X \to X'$ be a self-adjoint and positive operator. We define an inner product and its induced norm on X as follows:

$$(x,y)_{\mathcal{L}} = \langle \mathcal{L}(x), y\rangle, \qquad |||x|||_{\mathcal{L}} := \sqrt{(x,x)_{\mathcal{L}}} \quad \forall\, x, y \in X. \tag{3.11}$$

Let $\lambda := 1 + 24\kappa R_e(1+C_p^2)^2\,\|\boldsymbol{B}_n\|^2_{\boldsymbol{L}^\infty(\Omega)}$ be a parameter-dependent constant, and define

$$\mathcal{H}_0 = \operatorname{diag}\left(\kappa\mathcal{D}_J,\, \kappa\hat{\mathcal{I}}_\phi,\, \lambda\mathcal{F}_1,\, \lambda\mathcal{I}_p\right), \qquad \mathcal{H} = \mathcal{E}_1\mathcal{H}_0\mathcal{E}_1^*. \tag{3.12}$$

Let ζ_m be the approximate solution from the mth iteration of the GMRES method for solving the first equation of (3.10). Using the framework in [23, section 4.2], we get the convergence rate

$$\left|\!\left|\!\left|\mathcal{A}\hat{\mathcal{A}}^{-1}(\zeta-\zeta_m)\right|\!\right|\!\right|_{\mathcal{H}^{-1}} \le \sqrt{1 - C_{\inf}^2/C_{\sup}^2}\, \left|\!\left|\!\left|\mathcal{A}\hat{\mathcal{A}}^{-1}(\zeta-\zeta_{m-1})\right|\!\right|\!\right|_{\mathcal{H}^{-1}}, \tag{3.13}$$

where $C_{\inf}$, $C_{\sup}$ are positive constants such that

$$\inf_{\substack{\xi\in\boldsymbol{X}'\\ \xi\neq 0}} \frac{(\xi, (\mathcal{A}\hat{\mathcal{A}}^{-1})\xi)_{\mathcal{H}^{-1}}}{|||\xi|||^2_{\mathcal{H}^{-1}}} \ge C_{\inf}, \qquad \sup_{\substack{\xi\in\boldsymbol{X}'\\ \xi\neq 0}} \frac{\left|\!\left|\!\left|(\mathcal{A}\hat{\mathcal{A}}^{-1})\xi\right|\!\right|\!\right|_{\mathcal{H}^{-1}}}{|||\xi|||_{\mathcal{H}^{-1}}} \le C_{\sup}. \tag{3.14}$$

The estimates for $C_{\inf}$ and $C_{\sup}$ will be given in the following theorem.

THEOREM 3.2. *Suppose the stabilization parameter in* (3.1) *satisfies* $\alpha \ge 1$. *Then* (3.14) *holds with* $C_{\inf} = 1/4$ *and* $C_{\sup} = 2 + C_p^2$.

Proof. The proof is provided in Appendix B. ∎

Let ℓ_m be the approximate solution from the mth iteration of the GMRES method for solving the second equation of (3.10). Define

$$\hat{\mathcal{H}} = \operatorname{diag}\left(4\kappa\lambda C_p^2 \mathcal{D}_J,\ \kappa\lambda \mathcal{I}_\phi,\ \mathcal{F}_1,\ \mathcal{L}_p^{-1}\right).$$

Similarly we have the convergence rate

$$\left|\!\left|\!\left| \hat{\mathcal{A}}\mathcal{P}(\ell - \ell_m) \right|\!\right|\!\right|_{\hat{\mathcal{H}}^{-1}} \le \sqrt{1 - \hat{C}_{\inf}^2/\hat{C}_{\sup}^2}\ \left|\!\left|\!\left| \hat{\mathcal{A}}\mathcal{P}(\ell - \ell_{m-1}) \right|\!\right|\!\right|_{\hat{\mathcal{H}}^{-1}}, \tag{3.15}$$

where $\hat{C}_{\inf}$ and $\hat{C}_{\sup}$ are constants satisfying

$$\inf_{\substack{\xi \in \boldsymbol{X}' \\ \xi \neq 0}} \frac{(\xi, (\hat{\mathcal{A}}\mathcal{P})\xi)_{\hat{\mathcal{H}}^{-1}}}{|\!|\!|\xi|\!|\!|^2_{\hat{\mathcal{H}}^{-1}}} \ge \hat{C}_{\inf}, \qquad \sup_{\substack{\xi \in \boldsymbol{X}' \\ \xi \neq 0}} \frac{\left|\!\left|\!\left| (\hat{\mathcal{A}}\mathcal{P})\xi \right|\!\right|\!\right|_{\hat{\mathcal{H}}^{-1}}}{|\!|\!|\xi|\!|\!|_{\hat{\mathcal{H}}^{-1}}} \le \hat{C}_{\sup}. \tag{3.16}$$

THEOREM 3.3. *Define* $M := C_p^{1/2} R_e(\|\boldsymbol{u}_n^*\|_{\boldsymbol{L}^\infty(\Omega)} + \kappa C_p \|\boldsymbol{B}_n\|^2_{\boldsymbol{L}^\infty(\Omega)})$, *and let* $\alpha \ge 1$. *Assume* $\tau + \alpha_1^{-1} \le 8M^{-2}$ *for the time-dependent problem, or* $\alpha_1 \ge M^2$ *for the stationary problem. Then* (3.16) *holds with* $\hat{C}_{\inf} = 1/(4 + 4C_p^2)$ *and* $\hat{C}_{\sup} = 3$.

Proof. The proof is provided in Appendix C. ∎

Remark 3.4. We point out that the convergence in both (3.13) and (3.15) is not uniform with respect to the coupling number κ. In fact, since the two operators $\mathcal{H}_0$ and $\hat{\mathcal{H}}$ depend on κ, the norms $|\!|\!|\cdot|\!|\!|_{\mathcal{H}^{-1}}$ and $|\!|\!|\cdot|\!|\!|_{\hat{\mathcal{H}}^{-1}}$ also depend on κ. Therefore, the performance of the $\mathcal{P}$ preconditioner may be influenced by the variance of κ. We will show this statement numerically by Examples 5.1 and 5.3.

Remark 3.5. The assumptions for α and τ in Theorem 3.3 are not necessary in practical computations. Our numerical experiments show that the preconditioner works well for $\alpha = 1$ and moderate τ.

4. Algebraic preconditioner for the discrete problem. The purpose of this section is to propose a preconditioner for solving the linearized discrete problem (2.3) in each time step. The main idea is that, once a proper preconditioner is obtained for the continuous problem, and if the discretization of the continuous problem is stable, a robust preconditioner can be designed for the discrete problem by preserving the basic structure of the continuous preconditioner [23, 24]. To employ the continuous preconditioner in the previous section, we only consider the case of $\Gamma_{\mathrm{c}} = \Gamma_{\mathrm{n}} = \emptyset$ here. The preconditioner will be used directly in the cases of $\Gamma_{\mathrm{c}} \neq \emptyset$ and $\Gamma_{\mathrm{n}} \neq \emptyset$ in numerical computations.

The linear problem (2.3) can be written equivalently into an algebraic form,

$$\mathbb{A}\mathbf{x} = \mathbf{b}, \tag{4.1}$$

where $\mathbb{A}$ is the stiffness matrix, $\mathbf{x}$ is the vector of DOFs, and $\mathbf{b}$ is the load vector. In block form, they can be written as follows:

$$\mathbb{A} = \begin{pmatrix} \kappa\mathbb{M}_J & \kappa\mathbb{G}^\top & \kappa\mathbb{K}^\top & 0 \\ \kappa\mathbb{G} & 0 & 0 & 0 \\ -\kappa\mathbb{K} & 0 & \mathbb{F}_u & \mathbb{B}^\top \\ 0 & 0 & \mathbb{B} & 0 \end{pmatrix}, \quad \mathbf{x} = \begin{pmatrix} \mathbf{x}_J \\ \mathbf{x}_\phi \\ \mathbf{x}_u \\ \mathbf{x}_p \end{pmatrix}, \quad \mathbf{b} = \begin{pmatrix} \mathbf{b}_J \\ \mathbf{b}_\phi \\ \mathbf{b}_u \\ \mathbf{b}_p \end{pmatrix}. \tag{4.2}$$

Here $\mathbf{x}_J, \mathbf{x}_u, \mathbf{x}_\phi, \mathbf{x}_p$ are vectors of DOFs belonging to $\boldsymbol{J}_n$, $\bar{\boldsymbol{u}}_n$, ϕ_n, p_n, respectively, and $\mathbf{b}_J, \mathbf{b}_u, \mathbf{b}_\phi, \mathbf{b}_p$ are the corresponding load vectors. The submatrices $\mathbb{M}_J$, $\mathbb{G}$, $\mathbb{F}_u$,

$\mathbb{B}$, $\mathbb{K}$ are Galerkin matrices for the electric current term, the electric potential term, the fluid terms, the pressure term, and the coupling between $\bar{\boldsymbol{u}}_n$ and $\boldsymbol{J}_n$, namely,

$$\mathbb{M}_J \leftrightarrow (\boldsymbol{d}, \boldsymbol{d}'), \qquad \mathbb{G} \leftrightarrow -(\operatorname{div} \boldsymbol{d}, \varphi), \qquad \mathbb{K} \leftrightarrow (\boldsymbol{d}, \boldsymbol{B}_n \times \boldsymbol{v}'),$$

$$\mathbb{F}_u \leftrightarrow \frac{2}{\tau}(\boldsymbol{v}, \boldsymbol{v}') + \mathscr{O}(\boldsymbol{u}_n^*; \boldsymbol{v}, \boldsymbol{v}') + \mathscr{A}_{\mathrm{AL}}(\boldsymbol{v}, \boldsymbol{v}'), \qquad \mathbb{B} \leftrightarrow -(\operatorname{div} \boldsymbol{v}, q)$$

for all $\boldsymbol{d}, \boldsymbol{d}' \in \boldsymbol{D}_0 \cap \boldsymbol{D}^h$, $\boldsymbol{v}, \boldsymbol{v}' \in \boldsymbol{V}_0 \cap \boldsymbol{V}^h$, $\varphi \in S^h$, and $q \in Q^h$.

By (3.9), the direct preconditioner of $\mathbb{A}$ is the algebraic representation of $\mathcal{P}$. However, in view of (3.4), the term $\kappa \mathcal{K}^* \hat{\mathcal{I}}_J \mathcal{K}$ makes the computation of $\mathcal{F}_\kappa$ complicated. To save computations, we replace $\kappa \mathcal{K}^* \hat{\mathcal{I}}_J \mathcal{K}$ with $\kappa \mathcal{K}^* \mathcal{K}$ in $\mathcal{F}_\kappa$ and define matrix $\mathbb{F}_\kappa$ by the bilinear form $\langle \mathcal{F}_u \boldsymbol{v}, \boldsymbol{v}' \rangle + \kappa(\mathcal{K}\boldsymbol{v}, \mathcal{K}\boldsymbol{v}')$, namely,

$$\mathbb{F}_\kappa \leftrightarrow \frac{2}{\tau}(\boldsymbol{v}, \boldsymbol{v}') + \mathscr{O}(\boldsymbol{u}_n^*; \boldsymbol{v}, \boldsymbol{v}') + \mathscr{A}_{\mathrm{AL}}(\boldsymbol{v}, \boldsymbol{v}') + \kappa(\mathcal{K}\boldsymbol{v}, \mathcal{K}\boldsymbol{v}') \quad \forall\, \boldsymbol{v}, \boldsymbol{v}' \in \boldsymbol{V}_0 \cap \boldsymbol{V}^h.$$

This is reasonable. By Lemma A.2, $\hat{\mathcal{I}}_J$ is self-adjoint, positive, and bounded by the identity operator $\mathcal{I}_J$, namely,

$$\left\| \hat{\mathcal{I}}_J \boldsymbol{d} \right\|^2_{\boldsymbol{H}(\operatorname{div},\Omega)} = \left(\boldsymbol{d}, \hat{\mathcal{I}}_J \boldsymbol{d} \right) \le \|\boldsymbol{d}\|^2_{\boldsymbol{L}^2(\Omega)}.$$

Therefore, the right preconditioner for $\mathbb{A}$ is given by

$$\mathbb{P} = \begin{pmatrix} \kappa \mathbb{D}_J & 2\kappa \mathbb{G}^\top & 2\kappa \mathbb{K}^\top & 0 \\ 0 & -\kappa \mathbb{M}_\phi & 0 & 0 \\ 0 & 0 & \mathbb{F}_\kappa & \mathbb{B}^\top \\ 0 & 0 & 0 & -\mathbb{L}_p^{-1} \end{pmatrix}^{-1}, \tag{4.3}$$

where the submatrices of $\mathbb{P}^{-1}$ are defined by

$$\mathbb{D}_J \leftrightarrow (\boldsymbol{d}, \boldsymbol{d}') + (\operatorname{div} \boldsymbol{d}, \operatorname{div} \boldsymbol{d}'), \qquad \mathbb{M}_\phi \leftrightarrow (\varphi, \varphi'),$$

$$\mathbb{L}_p \leftrightarrow \alpha_1 \mathbb{M}_p^{-1} + \frac{2}{\tau} \mathbb{S}_p^{-1}, \qquad \mathbb{M}_p \leftrightarrow (q, q'), \qquad \mathbb{S}_p \leftrightarrow (\nabla q, \nabla q')$$

for all $\boldsymbol{d}, \boldsymbol{d}' \in \boldsymbol{D}_0 \cap \boldsymbol{D}^h$, $\varphi, \varphi' \in S^h$, and $q, q' \in Q^h$.

The preconditioning step needs to solve a system of algebraic equations,

$$\mathbb{P}\,\mathbf{y} = \mathbf{r}. \tag{4.4}$$

We present the algorithm for solving an approximate solution of (4.4). Write $\mathbf{y} = (\mathbf{y}_J, \mathbf{y}_\phi, \mathbf{y}_u, \mathbf{y}_p)^\top$ and $\mathbf{r} = (\mathbf{r}_J, \mathbf{r}_\phi, \mathbf{r}_u, \mathbf{r}_p)^\top$.

ALGORITHM 4.1. 1. Compute $\mathbf{y}_p = -\mathbb{L}_p \mathbf{r}_p = -\alpha_1 \boldsymbol{\xi} - \boldsymbol{\eta}$ where $\boldsymbol{\xi}$, $\boldsymbol{\eta}$ are solved in two steps [14]:

- solve $\mathbb{M}_p \boldsymbol{\xi} = \mathbf{r}_p$ by 10 iterations of CG solver with diagonal preconditioner,
- solve $\mathbb{S}_p \boldsymbol{\eta} = \mathbf{r}_p$ by two iterations of AMG solver (see [15]).

2. Solve $\mathbb{M}_\phi \mathbf{y}_\phi = -\mathbf{r}_\phi$ by 10 iterations of CG solver with diagonal preconditioner.

3. Solve $\mathbb{F}_\kappa \mathbf{y}_u = \mathbf{r}_u - \mathbb{B}^\top \mathbf{y}_p$ by GMRES solver with additive Schwarz preconditioner. The tolerance for relative residuals is set to 10^{-3}.

4. Solve $\mathbb{D}_J \mathbf{y}_J = \mathbf{r}_J - 2\mathbb{G}^\top \mathbf{y}_\phi - 2\mathbb{K}^\top \mathbf{y}_u$ by five CG iterations with the Hiptmair–Xu preconditioner [17].

In step 3 of Algorithm 4.1, each subdomain problem of the additive Schwarz method is solved by the MUMPS solver [26]. We also recommend using ILU solvers for subdomain problems [33, section 5]. For a stationary fluid problem with large Reynolds number, it is known that Newton's method converges faster than Picard's method (cf. [21]). However, by Newton's method, the linearized problem becomes more complicated, and it is difficult to prove the convergence rate of the preconditioned GMRES method. In [21], the authors studied the stationary problem of the full MHD equations and obtained a robust preconditioner for Newton's method. They simply replaced the linearized terms of Picard's method with those of Newton's method in preconditioning. We only consider Picard's method in this section. The results can be extended to Newton's method similarly as done in [21].

Remark 4.2. For enclosed flow where $\Gamma_{\mathrm{n}} = \emptyset$, assembling $\mathbb{S}_p$ does not need the Dirichlet boundary condition of p. However, for outflow boundary where $\Gamma_{\mathrm{n}} \neq \emptyset$ and the pressure is undetermined, $\mathbb{S}_p$ should be assembled on the subspace $\{q_h \in Q^h : q_h = 0 \text{ on } \Gamma_{\mathrm{n}}\}$.

5. Numerical results. In this section, we report three numerical experiments to show the quasi-optimality of the solver with respect to the number of DOFs. The finite element method and the discrete solver are implemented on the adaptive finite element package "Parallel Hierarchical Grid" (PHG) [40]. The objectives of these experiments are as follows:

- Example 5.1 shows the quasi-optimality of the stationary solver by computing a driven cavity flow with $\boldsymbol{J} \cdot \boldsymbol{n} = 0$ on Γ.
- Example 5.2 shows the quasi-optimality of the stationary solver by computing the driven cavity flow with $\phi = 0$ on Γ. We also investigate the sensitivity of the solver to the AL-stabilization parameter α and to the Reynolds number.
- Example 5.3 investigates the performance of the time-dependent MHD solver by computing a pipe flow, namely, $\Gamma_{\mathrm{n}} \neq \emptyset$.

Throughout this section, we use Picard's method to solve stationary MHD problems and use the linearized finite element scheme (2.3) to solve time-dependent MHD problems.

Given the approximate solution $\mathbf{x}^{(k)}$ at the kth step, the residual of (4.1) is defined by $\mathbf{r}^{(k)} = \mathbf{b} - \mathbb{A}\mathbf{x}^{(k)}$. The restart of the GMRES solver is set to 5. The iterations stop whenever the relative residual is less than a given tolerance ε, namely,

$$\left\|\mathbf{r}^{(k)}\right\| < \varepsilon \left\|\mathbf{r}^{(0)}\right\|. \tag{5.1}$$

Throughout this section, we set the AL-stabilization parameter to $\alpha = 1$, except for those examples which test the sensitivity of the solver to α.

Example 5.1 (stationary problem with insulating wall). This example tests the efficiency of the preconditioner for solving the stationary problem. The cavity region is $\Omega = (0,1)^3$, and the external force is set to $\boldsymbol{f} = 0$. The applied magnetic field is $\boldsymbol{B} = (0,0,1)^\top$. The boundary condition for velocity reads $\boldsymbol{u} = (v,0,0)^\top$ on Γ, where

$$v \in C^1(\bar{\Omega}), \quad v(x,y,1) = 1, \quad \text{and} \quad v(x,y,z) = 0 \quad \forall\, z \in [0, 1-h].$$

The boundary condition for current density reads $\boldsymbol{J} \cdot \boldsymbol{n} = 0$ on Γ.

We denote by $R_e = 10$, 100, and 500 the Reynolds number, by $\kappa = 10$ and 10^3 the coupling number, by 10^{-5} the relative tolerance for Picard's iterations, and by

TABLE 1
Meshes and number of DOFs. (Example 5.1*.)*

Mesh	h	DOFs of $(\boldsymbol{J}_h, \phi_h)$	DOFs of $(\boldsymbol{u}_h, p_h)$
$\mathcal{T}_1$	0.217	22,656	15,468
$\mathcal{T}_2$	0.108	176,640	112,724
$\mathcal{T}_3$	0.054	1,394,688	859,812
$\mathcal{T}_4$	0.027	11,083,776	6,714,692

TABLE 2
Quasi-optimality of the discrete solver for $\kappa = 10 : N_{\text{gmres}}$ (N_{picard})*. (Example* 5.1*.)*

Grid	$R_e = 10$	$R_e = 100$	$R_e = 500$
$\mathcal{T}_1$	29 (3)	40 (6)	71 (10)
$\mathcal{T}_2$	30 (3)	42 (6)	77 (12)
$\mathcal{T}_3$	30 (3)	43 (6)	80 (12)
$\mathcal{T}_4$	30 (3)	43 (6)	82 (12)

TABLE 3
Quasi-optimality of the discrete solver for $\kappa = 10^3 : N_{\text{gmres}}$ (N_{picard})*. (Example* 5.1*.)*

Grid	$R_e = 10$	$R_e = 100$	$R_e = 500$
$\mathcal{T}_1$	133 (3)	160 (3)	239 (3)
$\mathcal{T}_2$	133 (2)	178 (3)	251 (4)
$\mathcal{T}_3$	129 (2)	187 (3)	245 (5)
$\mathcal{T}_4$	128 (2)	192 (3)	248 (5)

$\varepsilon = 10^{-8}$ the relative tolerance for solving linear systems. The meshes are refined successively and uniformly such that the mesh size of $\mathcal{T}_l$ is given by

$$h_l = \sqrt{3} \times 2^{-l-2}, \qquad l = 1, 2, 3, 4.$$

The numbers of DOFs for all unknowns are listed in Table 1.

Table 2 shows the number of Picard's iterations (denoted by N_{picard}) and the average number of GMRES iterations (denoted by N_{gmres}) for solving the linear system (4.1) with $\kappa = 10$. For fixed Reynolds number R_e, N_{gmres} is quasi-uniform with respect to h and implies the quasi-optimality of the block preconditioner. When Re increases from 10 to 500, the number of GMRES iterations also increases mildly.

Table 3 shows the values of N_{gmres} and N_{picard} for $\kappa = 10^3$. We find that the N_{gmres} for $\kappa = 10^3$ is about 3–4 times larger than the N_{gmres} for $\kappa = 10$. As stated in Remark 3.4, the performance of the preconditioner can be influenced by κ. In view of (3.6) and (3.8), we have simply neglected the $(2,3)$-entry of $\hat{\mathcal{A}}$, that is, $\kappa \operatorname{div} \mathcal{D}_J^{-1}\mathcal{K}$, to precondition $\hat{\mathcal{A}}$ with $\mathcal{P}$. So the preconditioner does not embody the strong coupling between fluid and current density sufficiently for large κ. When $\kappa \operatorname{div} \mathcal{D}_J^{-1}\mathcal{K}$ is included in Algorithm 4.1, it needs to solve a coupled problem for $\mathbf{y}_\phi$ and $\mathbf{y}_J$ in steps 2 and 4, and this is more time-consuming. When R_e increases from 10 to 500, the number of GMRES iterations also increases mildly. However, for fixed R_e and κ, N_{gmres} is still quasi-uniform with respect to h and implies the quasi-optimality of the block preconditioner.

Example 5.2 (stationary problem with conducting wall). This example investigates the robustness of the preconditioner to Reynolds number R_e and the AL-stabilization parameter α. The setting is the same as that of Example 5.1, except that $\boldsymbol{B} = (1, 0, 0)^\top$ and $\phi|_\Gamma = 0$ are used.

TABLE 4
Average N_{gmres} required for reducing relative residual below 10^{-10}. Here "$\times$" means no convergence within 100 Picard iterations. (Example 5.2.)

R_e	Mesh	$\kappa = 1$	$\kappa = 10$
100	$\mathcal{T}_1$	22 (10)	35 (6)
	$\mathcal{T}_2$	23 (9)	37 (6)
	$\mathcal{T}_3$	24 (8)	38 (5)
	$\mathcal{T}_4$	24 (7)	39 (5)
200	$\mathcal{T}_1$	25 (16)	40 (7)
	$\mathcal{T}_2$	25 (17)	42 (7)
	$\mathcal{T}_3$	27 (16)	45 (6)
	$\mathcal{T}_4$	28 (15)	45 (6)
400	$\mathcal{T}_1$	28 (32)	47 (8)
	$\mathcal{T}_2$	29 (53)	50 (8)
	$\mathcal{T}_3$	30 (58)	52 (8)
	$\mathcal{T}_4$	29 (59)	52 (8)
800	$\mathcal{T}_1$	36 ($\times$)	53 (10)
	$\mathcal{T}_2$	39 ($\times$)	58 (12)
	$\mathcal{T}_3$	40 ($\times$)	62 (12)
	$\mathcal{T}_4$	40 ($\times$)	63 (11)

TABLE 5
The sensitivity of the discrete solver to α ($R_e = 400, \kappa = 10$). (Example 5.2.)

Meshes	$\alpha = 0$	$\alpha = 0.01$	$\alpha = 0.1$	$\alpha = 0.5$	$\alpha = 1$	$\alpha = 10$
$\mathcal{T}_1$	185 (12)	83 (9)	49 (8)	47 (8)	47 (8)	45 (8)
$\mathcal{T}_2$	202 (9)	85 (8)	53 (8)	50 (8)	50 (8)	50 (8)
$\mathcal{T}_3$	240 (8)	90 (8)	56 (8)	52 (8)	52 (8)	51 (8)

The tolerance for Picard's method is set to 10^{-5}, and the tolerance for the GMRES solver is set to $\varepsilon = 10^{-10}$. From Table 4, we find that the GMRES solver is robust to R_e and quasi-optimal to h. Particularly, for $R_e = 800$ and $\kappa = 1$, although Picard's method does not converge within 100 iterations due to strong convection, we can still obtain the quasi-optimality of the GMRES solver.

Next we investigate the sensitivity of the GMRES solver to AL-stabilization parameter α. Here we fix the Reynolds number to $R_e = 400$ and the coupling number to $\kappa = 10$. Table 5 shows that the discrete solver is robust and quasi-optimal for $\alpha \geq 0.1$.

Now we show the streamlines of discrete solutions generated by a line segment source

$$\left\{(0.5, 0.5, z)^\top : 0 \leq z \leq 1\right\}.$$

Figure 1 shows the streamlines of $\boldsymbol{u}_h$ for $\kappa = 1$ and $R_e = 100, 200, 400$, respectively. Figure 2 shows the streamlines of $\boldsymbol{u}_h$ for $\kappa = 10$ and $R_e = 100, 200, 400$, respectively. The streamlines of both $\boldsymbol{u}_h$ and $\boldsymbol{J}_h$ are depicted in Figure 3 for $\kappa = 10$ and $R_e = 800$. As the coupling number increases, the fluid yields larger vertices and tends to be stratified.

Example 5.3 (pipe flow). This example investigates the performance of the GMRES solver for the time-dependent MHD problem by computing a pipe flow with inflow and outflow boundaries. The pipe occupies a cuboid $\Omega = (0, 1) \times (0, 4) \times (0, 1)$. On the outflow boundary, we impose

$$\frac{1}{R_e}\frac{\partial \boldsymbol{u}}{\partial \boldsymbol{n}} = p\boldsymbol{n} \quad \text{on } \Gamma_{\text{out}} = \Gamma_{\text{n}} := \{(x, 4, z) : 0 < x, z < 1\}.$$

On the inflow boundary and on fixed walls, the following Dirichlet boundary conditions are imposed:

$$\begin{aligned} \boldsymbol{u} &= (0, g, 0)^\top \quad \text{on } \Gamma_{\text{in}} := \{(x, 0, z) : 0 < x, z < 1\}, \\ \boldsymbol{u} &= (0, 0, 0)^\top \quad \text{on } \Gamma_{\text{wall}} := \Gamma \backslash (\Gamma_{\text{in}} \cup \Gamma_{\text{out}}), \end{aligned}$$

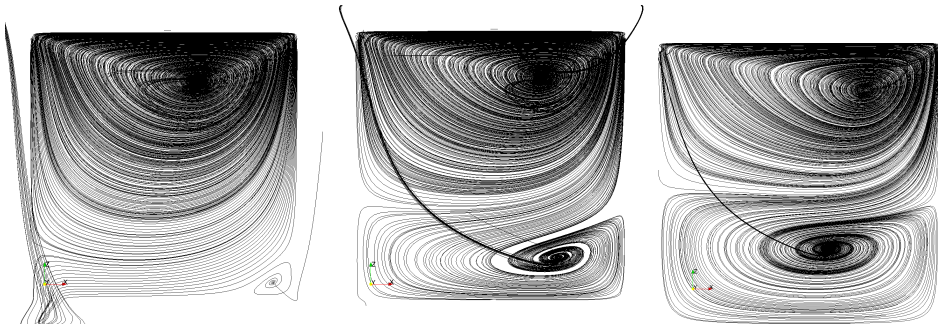

FIG. 1. *Streamlines of* $\boldsymbol{u}_h$ *for* $\kappa = 1$ *and* $R_e = 100, 200, 400$ *from left to right. (Example* 5.2*.)*

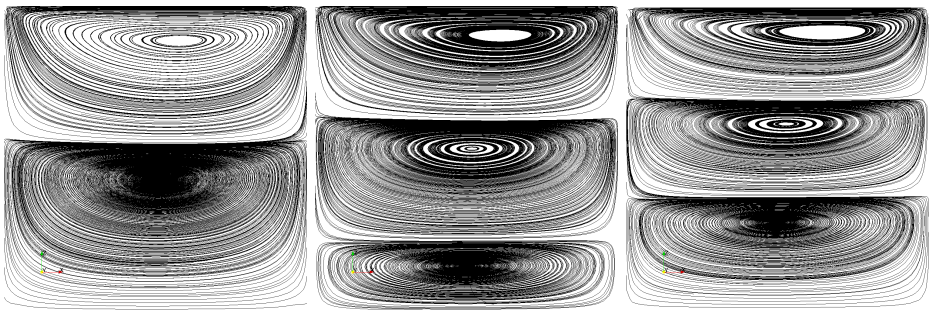

FIG. 2. *Streamlines f* $\boldsymbol{u}_h$ *for* $\kappa = 10$ *and* $R_e = 100, 200, 400$ *from left to right. (Example* 5.2*.)*

where $g = 10(1 - e^{-5t})(x^2 - x)(z^2 - z)$. The following insulating boundary condition is imposed:

$$\boldsymbol{J} \cdot \boldsymbol{n} = 0 \quad \text{on} \ \ \Gamma.$$

Moreover, the applied magnetic field is given by $\boldsymbol{B} = (b, 0, 0)^\top$ with

$$b(y) = \begin{cases} 0 & \text{if } \ y < 1 \ \text{ or } \ y > 3, \\ (y-1)(3-y) & \text{if } \ 1 \le y \le 3. \end{cases}$$

The relative tolerance for the GMRES solver is set to $\varepsilon = 10^{-6}$. Let $\mathcal{M}_1, \ldots, \mathcal{M}_4$ be four successively refined meshes whose sizes are $h_j \approx 0.433/j$, $j = 1, \ldots, 4$ (see Figure 4 for $\mathcal{M}_1$). The numbers of DOFs of discrete solutions are listed in Table 6. At $t_n = 1$, the maximal material velocity is given by $u_{\max} \approx \|g(t_n)\|_{L^\infty(\Omega)} \approx 0.625$. So the CFL condition for the material velocity requires

$$\tau \le h_j u_{\max}^{-1} \approx 1.6 h_j \quad \text{on} \ \ \mathcal{M}_j, \quad j = 1, \ldots, 4.$$

For the inductionless MHD model that is essentially parabolic, we only consider the characteristic time for magnetic braking for the fluid. For $\kappa = 10^3$, this requires

$$\tau \le \left(\kappa \, \|\boldsymbol{B}(t_n)\|^2_{\boldsymbol{L}^\infty(\Omega)} \right)^{-1} \approx 1/9000 \approx 1.1 \times 10^{-4}.$$

To test the robustness of the preconditioner, we only investigate the cases of $\tau = 0.1$ and $\tau = 0.01$, which are much larger than the two criteria for time steps. From

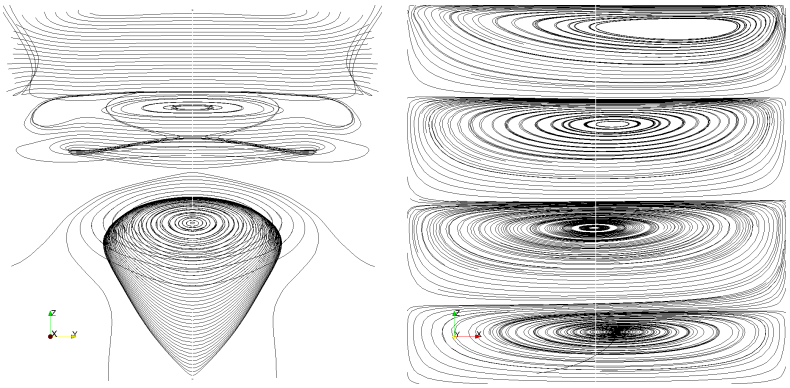

FIG. 3. *Streamlines of* $\boldsymbol{J}_h$ *(left) and streamlines of* $\boldsymbol{u}_h$ *(right) for* $\kappa = 10, R_e = 800$. *(Example* 5.2.*)*

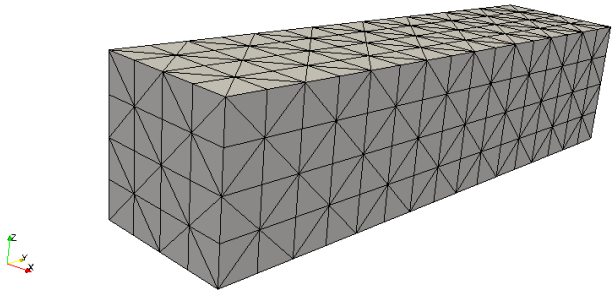

FIG. 4. *Tetrahedral mesh* $\mathcal{M}_1$ *of the pipe. (Example* 5.3.*)*

Table 7, we find that the discrete solver is not optimal when both κ and τ are large, say, $\kappa = 10^3$ and $\tau = 0.1$. This also happens in Example 5.1 for large κ and is mainly due to neglecting the $(2,3)$-entry of $\hat{\mathcal{A}}$ when designing the preconditioner. However, Table 8 shows that if we reduce the time step to $\tau = 0.01$, the quasi-optimality of the solver is obtained. Moreover, for fixed κ and τ, the solver is robust to the Reynolds number and quasi-optimal to the number of DOFs.

Next we fix the mesh $\mathcal{M}_4$ and investigate how the coupling number κ influences the fluid. The parameters are set to

$$R_e = 10^3, \qquad \kappa = 0,\ 10,\ 100, \qquad \tau = 0.01, \qquad t_N = T = 5.5, \qquad \alpha = 1,$$

The distributions of $|\boldsymbol{u}_N|$ are plotted in Figure 5. When the magnetic field is applied and is perpendicular to the direction of the pipe, the middle and lower figures show that the conducting fluid tends to slow down in the middle of the pipe and to flow out near the wall, compared with the nonconducting fluid (top figure).

Figure 6 shows the parallel component of the velocity in the direction of the pipe. It shows clearly that the parallel velocity decreases in the middle of the pipe as the coupling number increases.

TABLE 6
Numbers of DOFs of discrete solutions. (Example 5.3.)

Mesh	h	$(\boldsymbol{J}_n, \phi_n)$	$(\boldsymbol{u}_n, p_n)$
$\mathcal{M}_1$	0.433	11,616	8,444
$\mathcal{M}_2$	0.217	89,472	59,028
$\mathcal{M}_3$	0.108	701,952	440,228
$\mathcal{M}_4$	0.054	5,560,320	3,397,956

TABLE 7
The number of GMRES iterations for $\tau = 0.1$ and $t_n = 1.0$. (Example 5.3.)

R_e	Mesh	$\kappa = 10^2$	$\kappa = 10^3$
10^3	$\mathcal{M}_1$	34	95
	$\mathcal{M}_2$	32	105
	$\mathcal{M}_3$	32	131
	$\mathcal{M}_4$	30	148
10^4	$\mathcal{M}_1$	34	95
	$\mathcal{M}_2$	36	110
	$\mathcal{M}_3$	34	163
	$\mathcal{M}_4$	32	> 200

Figure 7 shows that the magnetic field also leads to inhomogeneous pressure of the conducting fluid. Higher pressure is concentrated in the middle region of the pipe where the fluid is forced by the magnetic field to change direction. Conversely, electric currents are influenced by the fluid dynamics. Figures 8 and 9 show that the current density becomes larger near the pipe wall where the fluid flows faster.

6. Conclusions. In this paper, we propose a robust preconditioner for solving the finite element discretization of inductionless MHD equations. The preconditioner is designed by using the framework of FOV-equivalence and block factorization of the coefficient matrix. By three numerical examples, we show that the preconditioner is robust to relatively large Reynolds number and quasi-optimal to the mesh size. The following are two important issues still to be studied in future work:

- The solution of the fluid convection-diffusion equation, that is, step 3 of Algorithm 4.1, is still not scalable in our code.
- The present preconditioner is not robust with respect to large coupling number κ. Better approximation to the $(2,3)$-entry of $\hat{\mathcal{A}}$ should be studied when designing the preconditioner.

Appendix A. Useful estimates for linear operators. The purpose of this appendix is to prove some useful results which will be used in the proofs of Theorems 3.2 and 3.3.

LEMMA A.1. *The operator $\hat{\mathcal{I}}_\phi := -\operatorname{div} \mathcal{D}_J^{-1} \nabla$ is self-adjoint and positive on S. For $\xi \in S$,*

$$\left(1 + C_p^2\right)^{-1} \|\xi\|_{L^2(\Omega)} \le \left\| \hat{\mathcal{I}}_\phi \xi \right\|_{L^2(\Omega)} \le \|\xi\|_{L^2(\Omega)}, \tag{A.1}$$

$$\left(1 + C_p^2\right)^{-1} \|\xi\|_{L^2(\Omega)}^2 \le \left(\hat{\mathcal{I}}_\phi \xi, \xi\right) \le \|\xi\|_{L^2(\Omega)}^2, \tag{A.2}$$

where C_p is the the Poincaré constant in (3.7).

Proof. It is easy to see that $\hat{\mathcal{I}}_\phi$ is a self-adjoint operator on S. The formula of integration by parts implies that $\hat{\boldsymbol{w}} := \mathcal{D}_J^{-1}(\nabla \xi)$ satisfies

$$(\hat{\boldsymbol{w}}, \boldsymbol{a}) + (\operatorname{div} \hat{\boldsymbol{w}}, \operatorname{div} \boldsymbol{a}) = \langle \nabla \xi, \boldsymbol{a} \rangle = -(\xi, \operatorname{div} \boldsymbol{a}) \quad \forall\, \boldsymbol{a} \in \boldsymbol{D}_0. \tag{A.3}$$

TABLE 8
The number of GMRES iterations for $\tau = 0.01$ and $t_n = 1.0$. (Example 5.3.)

R_e	Mesh	$\kappa = 10^2$	$\kappa = 10^3$
10^3	$\mathcal{M}_1$	19	37
	$\mathcal{M}_2$	17	37
	$\mathcal{M}_3$	17	39
	$\mathcal{M}_4$	18	39
10^4	$\mathcal{M}_1$	18	35
	$\mathcal{M}_2$	17	37
	$\mathcal{M}_3$	17	40
	$\mathcal{M}_4$	18	45

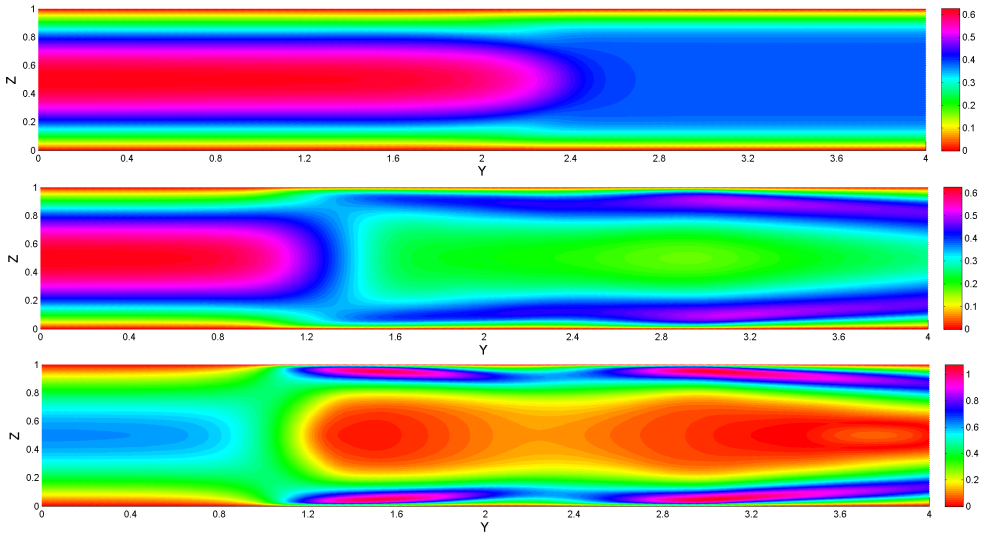

FIG. 5. *The distributions of $|\boldsymbol{u}_n|$ at cross-section $x = 0.5$ ($\kappa = 0$, 10, 100). (Example 5.3.)*

Clearly $\left(\hat{\mathcal{I}}_\phi \xi, \xi\right) = \|\hat{\boldsymbol{w}}\|^2_{\boldsymbol{H}(\mathrm{div},\Omega)}$. So $\hat{\mathcal{I}}_\phi$ is also positive.

Let $u \in H^1(\Omega)/\mathbb{R}$ be the solution of the elliptic equation

$$(\nabla u, \nabla v) = (\xi, v) \quad \forall\, v \in H^1(\Omega)/\mathbb{R}.$$

This indicates that $\boldsymbol{w} := \nabla u \in \boldsymbol{H}_0(\mathrm{div}, \Omega)$ and $\mathrm{div}\, \boldsymbol{w} = -\xi \in S$. Taking $\boldsymbol{a} = \hat{\boldsymbol{w}}$ in (A.3) yields

$$\left\|\hat{\mathcal{I}}_\phi \xi\right\|_{L^2(\Omega)} = \|\mathrm{div}\, \hat{\boldsymbol{w}}\|_{L^2(\Omega)} \le \|\xi\|_{L^2(\Omega)}\,.$$

Taking $\boldsymbol{a} = -\boldsymbol{w}$ in (A.3) and using $\mathrm{div}\, \hat{\boldsymbol{w}} = -\hat{\mathcal{I}}_\phi \xi$ lead to

$$\|\xi\|^2_{L^2(\Omega)} = -(\hat{\boldsymbol{w}}, \boldsymbol{w}) + (\mathrm{div}\, \hat{\boldsymbol{w}}, \xi) = (\mathrm{div}\, \hat{\boldsymbol{w}}, u + \xi) \le (1 + C_p^2) \left\|\hat{\mathcal{I}}_\phi \xi\right\|_{L^2(\Omega)} \|\xi\|_{L^2(\Omega)}\,.$$

This proves (A.1).

From (3.11), $\hat{\mathcal{I}}_\phi$ provides an inner product $(\cdot,\cdot)_{\hat{\mathcal{I}}_\phi}$ and a norm $|||\cdot|||_{\hat{\mathcal{I}}_\phi}$ on S. Using Schwarz's inequality and (A.1), we find that

$$(\xi,\xi) = \left(\hat{\mathcal{I}}_\phi^{-1}\xi, \xi\right)_{\hat{\mathcal{I}}_\phi} \le \left\|\left\|\hat{\mathcal{I}}_\phi^{-1}\xi\right\|\right\|_{\hat{\mathcal{I}}_\phi} |||\xi|||_{\hat{\mathcal{I}}_\phi} = \left(\hat{\mathcal{I}}_\phi^{-1}\xi, \xi\right)^{1/2} |||\xi|||_{\hat{\mathcal{I}}_\phi} \le (1 + C_p^2)^{1/2} \|\xi\|_{L^2(\Omega)} |||\xi|||_{\hat{\mathcal{I}}_\phi}.$$

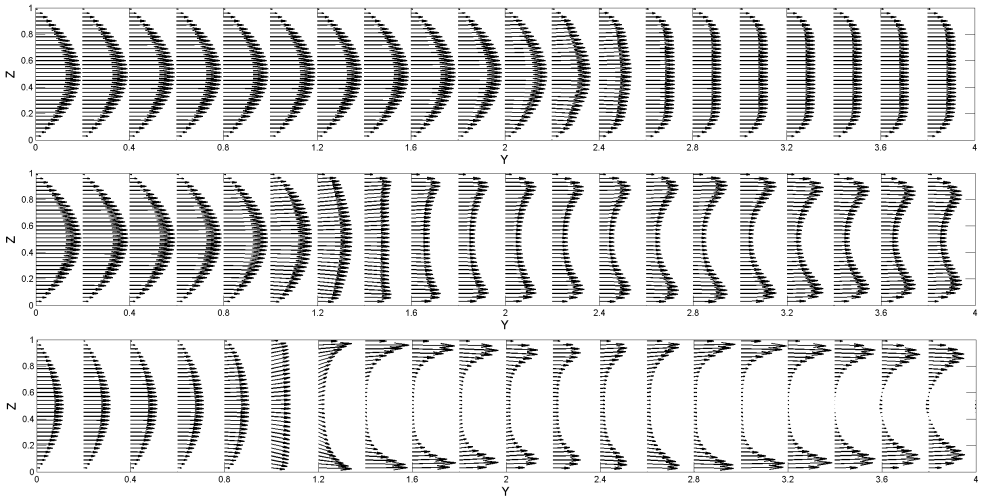

FIG. 6. *The x-component of $\boldsymbol{u}_n$ at cross-section $x = 0.5$ ($\kappa = 0$, 10, 100). (Example 5.3.)*

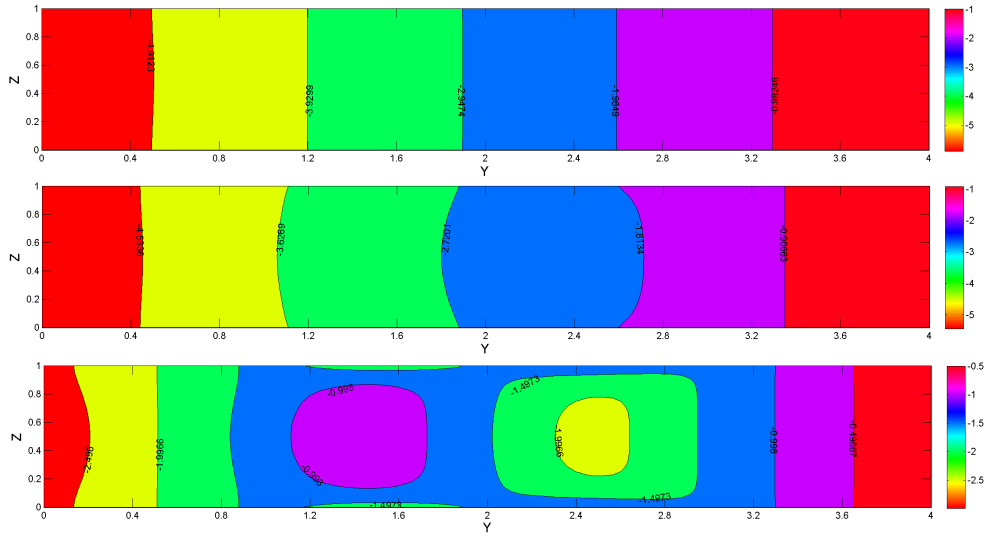

FIG. 7. *The distributions of p_n at cross-section $x = 0.5$ ($\kappa = 0$, 10, 100). (Example 5.3.)*

It follows that

$$(1 + C_p^2)^{-1} \|\xi\|^2_{L^2(\Omega)} \le |||\xi|||^2_{\hat{\mathcal{I}}_\phi} = \left(\hat{\mathcal{I}}_\phi \xi, \xi\right) \le \left\|\hat{\mathcal{I}}_\phi \xi\right\|_{L^2(\Omega)} \|\xi\|_{L^2(\Omega)} \le \|\xi\|^2_{L^2(\Omega)}.$$

This proves (A.2). The proof is completed. ∎

LEMMA A.2. *The operator $\hat{\mathcal{I}}_J$ is self-adjoint and satisfies*

$$\left\|\hat{\mathcal{I}}_J \boldsymbol{d}\right\|^2_{\mathcal{D}_J} = \left(\boldsymbol{d}, \hat{\mathcal{I}}_J \boldsymbol{d}\right) = |||\boldsymbol{d}|||^2_{\mathcal{D}_J^{-1}} - \left\|\nabla(\hat{\mathcal{I}}_\phi^{-1} \operatorname{div} \mathcal{D}_J^{-1} \boldsymbol{d})\right\|^2_{\mathcal{D}_J^{-1}} \quad \forall\, \boldsymbol{d} \in \boldsymbol{D}_0'.$$

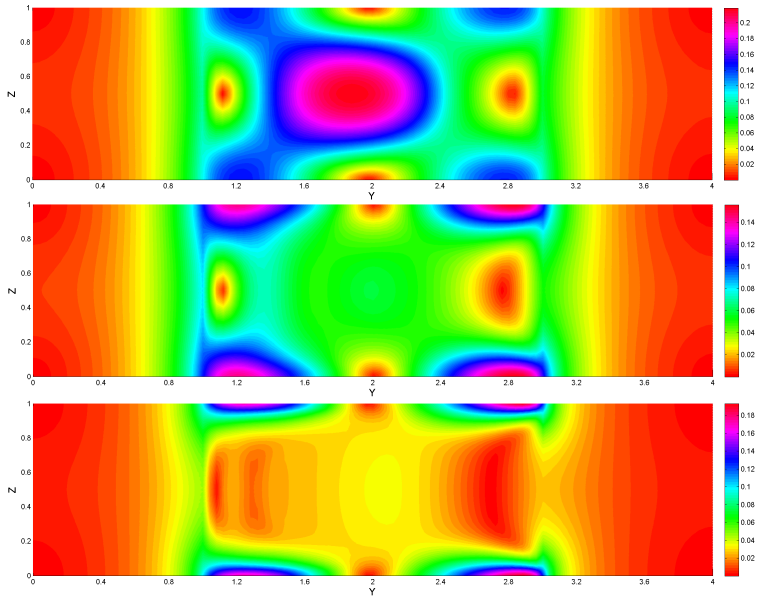

FIG. 8. *The distributions of* $|\boldsymbol{J}_n|$ *at cross-section* $x = 0.5$ ($\kappa = 0,\ 10,\ 100$). *(Example* 5.3.*)*

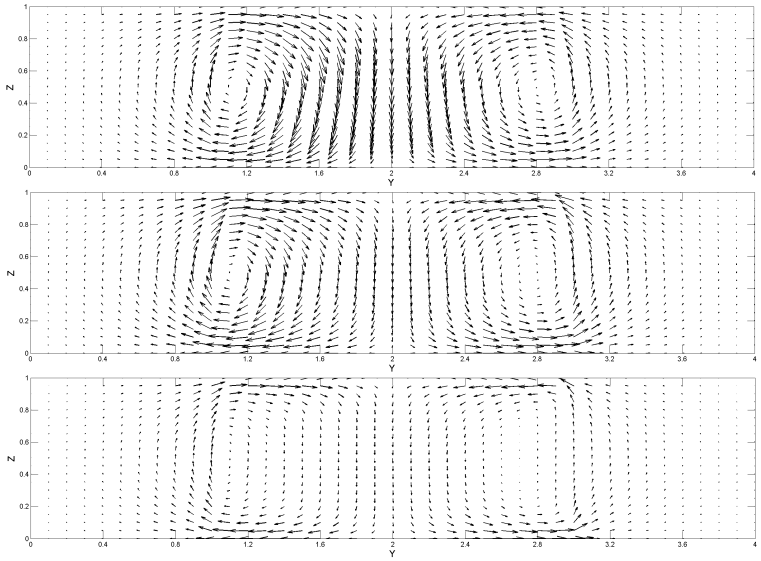

FIG. 9. *The* x*-component of* $\boldsymbol{J}_n$ *at cross-section* $x = 0.5$ ($\kappa = 0,\ 10,\ 100$). *(Example* 5.3.*)*

Proof. Define $\psi = \hat{\mathcal{I}}_\phi^{-1}\,\mathrm{div}(\mathcal{D}_J^{-1}\boldsymbol{d})$. From (3.4), we have $\hat{\mathcal{I}}_J\boldsymbol{d} = \mathcal{D}_J^{-1}(\boldsymbol{d}+\nabla\psi)$ and

$$\begin{aligned}
&\left\langle \mathcal{D}_J^{-1}(\nabla\psi), \nabla\psi\right\rangle = \left\langle \hat{\mathcal{I}}_\phi\psi, \psi\right\rangle = \left\langle \mathrm{div}(\mathcal{D}_J^{-1}\boldsymbol{d}), \psi\right\rangle = -\left\langle \mathcal{D}_J^{-1}\boldsymbol{d}, \nabla\psi\right\rangle,\\
&\left|\!\left|\!\left| \hat{\mathcal{I}}_J\boldsymbol{d}\right|\!\right|\!\right|_{\mathcal{D}_J}^2 = \left\langle \mathcal{D}_J^{-1}(\boldsymbol{d}+\nabla\psi), \boldsymbol{d}+\nabla\psi\right\rangle = \langle \mathcal{D}_J^{-1}\boldsymbol{d}, \boldsymbol{d}\rangle - \langle \mathcal{D}_J^{-1}(\nabla\psi), \nabla\psi\rangle,\\
&\left(\boldsymbol{d}, \hat{\mathcal{I}}_J\boldsymbol{d}\right) = \left(\mathcal{D}_J^{-1}\boldsymbol{d}, \boldsymbol{d}\right) + \left\langle \mathcal{D}_J^{-1}\boldsymbol{d}, \nabla\psi\right\rangle = \langle \mathcal{D}_J^{-1}\boldsymbol{d}, \boldsymbol{d}\rangle - \langle \mathcal{D}_J^{-1}(\nabla\psi), \nabla\psi\rangle.
\end{aligned}$$

The proof is completed. ∎

LEMMA A.3. *Assume* $\operatorname{div} \boldsymbol{u}_n^* = 0$. *Then for any* $\boldsymbol{v} \in \boldsymbol{V}_0$ *and* $\boldsymbol{\xi} \in \boldsymbol{V}_0'$,

$$\langle \mathcal{F}_\kappa \boldsymbol{v}, \boldsymbol{v} \rangle = |||\boldsymbol{v}|||_{\mathcal{F}_1}^2, \qquad |||\mathcal{F}_\kappa^{-1}\boldsymbol{\xi}|||_{\mathcal{F}_1} \le |||\mathcal{F}_1^{-1}\boldsymbol{\xi}|||_{\mathcal{F}_1}.$$

Proof. Since $\operatorname{div} \boldsymbol{u}_n^* = 0$, integration by parts implies $(\boldsymbol{u}_n^* \cdot \nabla \boldsymbol{v}, \boldsymbol{v}) = 0$ for any $\boldsymbol{v} \in \boldsymbol{V}_0$. This shows $\langle \mathcal{F}_\kappa \boldsymbol{v}, \boldsymbol{v} \rangle = \langle \mathcal{F}_1 \boldsymbol{v}, \boldsymbol{v} \rangle = |||\boldsymbol{v}|||_{\mathcal{F}_1}^2$. Moreover,

$$|||\mathcal{F}_\kappa^{-1}\boldsymbol{\xi}|||_{\mathcal{F}_1}^2 = \langle \boldsymbol{\xi}, \mathcal{F}_\kappa^{-1}\boldsymbol{\xi} \rangle \le |||\boldsymbol{\xi}|||_{\mathcal{F}_1^{-1}} |||\mathcal{F}_\kappa^{-1}\boldsymbol{\xi}|||_{\mathcal{F}_1} = |||\mathcal{F}_1^{-1}\boldsymbol{\xi}|||_{\mathcal{F}_1} |||\mathcal{F}_\kappa^{-1}\boldsymbol{\xi}|||_{\mathcal{F}_1}.$$

The proof is completed. ∎

LEMMA A.4. *Let* M *be defined in Theorem* 3.3, *and let the assumptions of Theorem* 3.3 *be satisfied. Then for any* $q \in Q$,

$$\left\|\left(\operatorname{div}\mathcal{F}_\kappa^{-1}\nabla + \mathcal{L}_p^{-1}\right) q\right\|_{L^2(\Omega)} \le M \left\|\mathcal{L}_p^{-1} q\right\|_{L^2(\Omega)} \times \begin{cases} \left(\tau + \alpha_1^{-1}\right)^{1/2} & \textit{time-dependent case,} \\ 3\alpha_1^{-1/2} & \textit{stationary case.} \end{cases}$$

Proof. Since $q = (\alpha_1 \mathcal{I}_p - 2\tau^{-1}\Delta_p^{-1})(\mathcal{L}_p^{-1} q)$, we find that

(A.4)
$$\|q\|_{L^2(\Omega)} \le \alpha_1 \left\|\mathcal{L}_p^{-1} q\right\|_{L^2(\Omega)} + 2\tau^{-1} \left\|\Delta_p^{-1}(\mathcal{L}_p^{-1} q)\right\|_{L^2(\Omega)} \le \left(\alpha_1 + 2C_p\tau^{-1}\right) \left\|\mathcal{L}_p^{-1} q\right\|_{L^2(\Omega)}.$$

Note that Δ_p, $\mathcal{L}_p$ are commutative, and $\operatorname{div} \mathcal{F}_\kappa = -\mathcal{L}_p \Delta_p \operatorname{div} + \operatorname{div}(\boldsymbol{u}_n^* \cdot \nabla + \kappa \mathcal{K}^* \hat{\mathcal{I}}_J \mathcal{K})$. Multiplying the equality by $\mathcal{F}_\kappa^{-1}\nabla$ from the right and by $\mathcal{L}_p^{-1}\Delta_p^{-1}$ from the left, we get

$$\eta := \left(\operatorname{div}\mathcal{F}_\kappa^{-1}\nabla + \mathcal{L}_p^{-1}\right) q = \mathcal{L}_p^{-1}\Delta_p^{-1} \operatorname{div}(\boldsymbol{u}_n^* \cdot \nabla + \kappa \mathcal{K}^* \hat{\mathcal{I}}_J \mathcal{K}) \mathcal{F}_\kappa^{-1}(\nabla q). \tag{A.5}$$

Write $\boldsymbol{w} = \mathcal{F}_\kappa^{-1}(\nabla q)$ and $\boldsymbol{\xi} = (\boldsymbol{u}_n^* \cdot \nabla + \kappa \mathcal{K}^* \hat{\mathcal{I}}_J \mathcal{K})\boldsymbol{w}$. By Lemma A.3, we have

$$|||\boldsymbol{w}|||_{\mathcal{F}_1}^2 = \langle \boldsymbol{w}, \mathcal{F}_\kappa \boldsymbol{w} \rangle = -(\operatorname{div} \boldsymbol{w}, q) \le \|\operatorname{div} \boldsymbol{w}\|_{L^2(\Omega)} \|q\|_{L^2(\Omega)}.$$

By Lemma A.2, $\boldsymbol{\xi}$ can be estimated as follows:

$$\begin{aligned} \|\boldsymbol{\xi}\|_{\boldsymbol{L}^2(\Omega)} &\le \|\boldsymbol{u}_n^* \cdot \nabla \boldsymbol{w}\|_{\boldsymbol{L}^2(\Omega)} + \kappa \|\mathcal{K}^* \mathcal{K} \boldsymbol{w}\|_{\boldsymbol{L}^2(\Omega)} \\ &\le \left(\|\boldsymbol{u}_n^*\|_{\boldsymbol{L}^\infty(\Omega)} + \kappa C_p \|\boldsymbol{B}_n\|_{\boldsymbol{L}^\infty(\Omega)}^2\right) |\boldsymbol{w}|_{\boldsymbol{H}^1(\Omega)} \\ &\le C_p^{-1/2} M |||\boldsymbol{w}|||_{\mathcal{F}_1} \le C_p^{-1/2} M \|\operatorname{div} \boldsymbol{w}\|_{L^2(\Omega)}^{1/2} \|q\|_{L^2(\Omega)}^{1/2}. \end{aligned} \tag{A.6}$$

Now we prove the lemma for the time-dependent case and the stationary case, respectively.

Case 1: Time-dependent case. Assume $0 < \tau \le 1$ without loss of generality. By (A.5), we have $2\tau^{-1}\eta - \alpha_1 \Delta_p \eta = -\operatorname{div} \boldsymbol{\xi}$. This implies

$$\frac{2}{\tau} \|\eta\|_{L^2(\Omega)}^2 + \alpha_1 |\eta|_{H^1(\Omega)}^2 = (\boldsymbol{\xi}, \nabla \eta) \le \frac{1}{4\alpha_1} \|\boldsymbol{\xi}\|_{\boldsymbol{L}^2(\Omega)}^2 + \alpha_1 |\eta|_{H^1(\Omega)}^2.$$

Using (A.4), (A.6), and the fact that $\operatorname{div} \boldsymbol{w} = \eta - \mathcal{L}_p^{-1}(q)$, we get

$$\begin{aligned} \|\eta\|_{L^2(\Omega)}^2 &\le \frac{\tau}{8\alpha_1} \|\boldsymbol{\xi}\|_{\boldsymbol{L}^2(\Omega)}^2 \le \frac{1}{4} M^2 (\alpha_1^{-1} + \tau) \left(\|\eta\|_{L^2(\Omega)} + \left\|\mathcal{L}_p^{-1} q\right\|_{L^2(\Omega)}\right) \left\|\mathcal{L}_p^{-1} q\right\|_{L^2(\Omega)} \\ &\le \frac{1}{2} \|\eta\|_{L^2(\Omega)}^2 + \frac{1}{32} M^2 (\alpha_1^{-1} + \tau) \left[8 + M^2 (\alpha_1^{-1} + \tau)\right] \left\|\mathcal{L}_p^{-1} q\right\|_{L^2(\Omega)}^2. \end{aligned}$$

Since $M^2(\tau+\alpha_1^{-1}) \le 8$ by the assumptions of Theorem 3.3, this leads to

$$\|\eta\|_{L^2(\Omega)} \le M\left(\tau+\alpha_1^{-1}\right)^{1/2}\left\|\mathcal{L}_p^{-1}q\right\|_{L^2(\Omega)}.$$

Case 2: Stationary case. In this case, we have $\tau=+\infty$ and $\mathcal{L}_p=\alpha_1\mathcal{I}_p$. Using (A.6) and the stability of the solution of Poisson's equation, we have

$$\left|\Delta_p^{-1}(\operatorname{div}\boldsymbol{\xi})\right|_{H^1(\Omega)} \le \|\boldsymbol{\xi}\|_{L^2(\Omega)} \le C_p^{-1/2}M\|\operatorname{div}\boldsymbol{w}\|_{L^2(\Omega)}^{1/2}\|q\|_{L^2(\Omega)}^{1/2}.$$

Together with (A.4) and $\operatorname{div}\boldsymbol{w}=\eta-\mathcal{L}_p^{-1}(q)$, this shows

$$\begin{aligned}\|\eta\|_{L^2(\Omega)}^2 &= \alpha_1^{-2}\left\|\Delta_p^{-1}(\operatorname{div}\boldsymbol{\xi})\right\|_{L^2(\Omega)}^2 \le \alpha_1^{-2}C_p^{-1}M^2\|\operatorname{div}\boldsymbol{w}\|_{L^2(\Omega)}\|q\|_{L^2(\Omega)}\\ &\le \frac{1}{2}\|\eta\|_{L^2(\Omega)}^2 + 2M^2\alpha_1^{-1}\left(1+M^2\alpha_1^{-1}\right)\left\|\mathcal{L}_p^{-1}q\right\|_{L^2(\Omega)}^2.\end{aligned}$$

Since $M^2\alpha_1^{-1}\le 1$ by the assumptions of Theorem 3.3, we get

$$\|\eta\|_{L^2(\Omega)} \le 3M\alpha_1^{-1/2}\left\|\mathcal{L}_p^{-1}q\right\|_{L^2(\Omega)}. \tag{A.7}$$

∎

Appendix B. The proof of Theorem 3.2.

Proof. For any $\xi\in\boldsymbol{X}'$, write $\Psi=(\mathcal{H}_0^{-1}\mathcal{E}_1^{-1})\xi$ and $\Phi=(\mathcal{H}_0^{-1}\mathcal{E}_2\mathcal{H}_0)\Psi$ for convenience. Since

$$\mathcal{H}^{-1}(\mathcal{A}\hat{\mathcal{A}}^{-1}) = (\mathcal{E}_1^*)^{-1}\mathcal{H}_0^{-1}\mathcal{E}_1^{-1}(\mathcal{E}_1\mathcal{E}_2\mathcal{E}_1^{-1}) = (\mathcal{E}_1^*)^{-1}\mathcal{H}_0^{-1}\mathcal{E}_2\mathcal{E}_1^{-1}, \tag{B.1}$$

it is easy to see that

$$(\xi,\mathcal{A}\hat{\mathcal{A}}^{-1}\xi)_{\mathcal{H}^{-1}} = \langle\Psi,\mathcal{E}_2\mathcal{H}_0\Psi\rangle, \quad |||\xi|||_{\mathcal{H}^{-1}}^2 = |||\Psi|||_{\mathcal{H}_0}^2, \quad \left|\left|\left|(\mathcal{A}\hat{\mathcal{A}}^{-1})\xi\right|\right|\right|_{\mathcal{H}^{-1}}^2 = |||\Phi|||_{\mathcal{H}_0}^2. \tag{B.2}$$

For convenience, we write

$$\begin{cases}\Psi=(\Psi_J,\Psi_\phi,\Psi_u,\Psi_p), & \Psi_J\in\boldsymbol{D}_0,\ \ \Psi_\phi\in S,\ \ \Psi_u\in\boldsymbol{V}_0,\ \ \Psi_p\in Q,\\ \hat{\Psi}_J:=\Psi_J+\mathcal{D}_J^{-1}(\nabla\Psi_\phi), & \hat{\Psi}_u:=\mathcal{F}_\kappa^{-1}\mathcal{F}_1\Psi_u.\end{cases} \tag{B.3}$$

The proof consists of two parts. Part I proves the inf-condition, that is, the first inequality of (3.14), and Part II proves the sup-condition, that is, the second inequality.

Part I: The inf-condition. Direct calculations show that

$$\langle\Psi,\mathcal{E}_2\mathcal{H}_0\Psi\rangle - |||\Psi|||_{\mathcal{H}_0}^2 = -\kappa(\operatorname{div}\Psi_J,\Psi_\phi) - \kappa\left\langle\hat{\Psi}_J,\mathcal{K}\Psi_u\right\rangle - \lambda(\operatorname{div}\hat{\Psi}_u,\Psi_p). \tag{B.4}$$

By Schwarz's inequality, the first term on the right-hand side of (B.4) satisfies

$$\kappa\left|(\operatorname{div}\Psi_J,\Psi_\phi)\right| \le \kappa\|\operatorname{div}\Psi_J\|_{L^2(\Omega)}\|\Psi_\phi\|_{L^2(\Omega)} \le \frac{\kappa}{2}\left(\|\operatorname{div}\Psi_J\|_{L^2(\Omega)}^2+\|\Psi_\phi\|_{L^2(\Omega)}^2\right).$$

By the definition of $\mathcal{K}$ and Poincaré's inequality, we have

$$\|\mathcal{K}\Psi_u\|_{\boldsymbol{L}^2(\Omega)} \le C_p\|\boldsymbol{B}_n\|_{\boldsymbol{L}^\infty}|\Psi_u|_{\boldsymbol{H}^1(\Omega)} \le C_pR_e^{1/2}\|\boldsymbol{B}_n\|_{\boldsymbol{L}^\infty}|||\Psi_u|||_{\mathcal{F}_1}. \tag{B.5}$$

The second term satisfies

$$\kappa\left|\langle\hat{\Psi}_J,\mathcal{K}\Psi_u\rangle\right|\le\kappa\left\|\hat{\Psi}_J\right\|_{\boldsymbol{L}^2(\Omega)}\|\mathcal{K}\Psi_u\|_{\boldsymbol{L}^2(\Omega)}\le\frac{\kappa}{4}|||\Psi_J|||^2_{\mathcal{D}_J}+\frac{\kappa}{4}\|\Psi_\phi\|^2_{L^2(\Omega)}+\frac{\lambda}{12}|||\Psi_u|||^2_{\mathcal{F}_1}.$$

Moreover, Lemma A.3 implies $\left|\left|\left|\hat{\Psi}_u\right|\right|\right|_{\mathcal{F}_1}\le|||\Psi_u|||_{\mathcal{F}_1}$. So the third term satisfies

$$\left|\lambda(\operatorname{div}\hat{\Psi}_u,\Psi_p)\right|\le\frac{\lambda}{\sqrt{\alpha}}\left|\left|\left|\hat{\Psi}_u\right|\right|\right|_{\mathcal{F}_1}\|\Psi_p\|_{L^2(\Omega)}\le\frac{\lambda}{2\alpha}|||\Psi_u|||^2_{\mathcal{F}_1}+\frac{\lambda}{2}\|\Psi_p\|^2_{L^2(\Omega)}.$$

Combining the above estimates yields an upper bound for the right-hand side of (B.4),

$$\begin{aligned}&\left|\kappa(\operatorname{div}\Psi_J,\Psi_\phi)+\kappa\langle\hat{\Psi}_J,\mathcal{K}\Psi_u\rangle+\lambda(\operatorname{div}\hat{\Psi}_u,\Psi_p)\right|\\&\qquad\le\frac{\lambda}{\alpha}|||\Psi_u|||^2_{\mathcal{F}_1}+\frac{\lambda}{4}\|\Psi_p\|^2_{L^2(\Omega)}+\frac{3\kappa}{4}\left(|||\Psi_J|||^2_{\mathcal{D}_J}+\|\Psi_\phi\|^2_{L^2(\Omega)}\right).\end{aligned}$$

Remembering $\alpha\ge1$ from the assumption, we get

$$\left|\kappa(\operatorname{div}\Psi_J,\Psi_\phi)+\kappa\langle\hat{\Psi}_J,\mathcal{K}\Psi_u\rangle+\lambda(\operatorname{div}\hat{\Psi}_u,\Psi_p)\right|\le\frac{3}{4}|||\Psi|||^2_{\mathcal{H}_0}. \tag{B.6}$$

Substituting (B.6) into (B.4) yields, for any $\xi\in\boldsymbol{X}'$,

$$(\xi,\mathcal{A}\hat{\mathcal{A}}^{-1}\xi)_{\mathcal{H}^{-1}}=\langle\Psi,\mathcal{E}_2\mathcal{H}_0\Psi\rangle\ge\frac{1}{4}|||\Psi|||^2_{\mathcal{H}_0}=\frac{1}{4}|||\xi|||^2_{\mathcal{H}^{-1}}. \tag{B.7}$$

Part II: The sup-condition. Direct calculations show that

$$\begin{aligned}|||\Phi|||^2_{\mathcal{H}_0}-|||\Psi|||^2_{\mathcal{H}_0}=&-2\kappa(\Psi_\phi,\operatorname{div}\Psi_J)-2\kappa\left\langle\mathcal{K}\Psi_u,\hat{\Psi}_J\right\rangle-2\lambda(\Psi_p,\operatorname{div}\hat{\Psi}_u)\\&+\kappa|||\operatorname{div}\Psi_J|||^2_{\hat{\mathcal{I}}_\phi^{-1}}+\lambda\left\|\operatorname{div}\hat{\Psi}_u\right\|^2_{L^2(\Omega)}+\frac{\kappa^2}{\lambda}\left|\left|\left|\mathcal{K}^*\hat{\Psi}_J\right|\right|\right|^2_{\mathcal{F}_1^{-1}}.\end{aligned} \tag{B.8}$$

Using Lemma A.1 and $\left|\left|\left|\hat{\Psi}_u\right|\right|\right|^2_{\mathcal{F}_1}\le|||\Psi_u|||^2_{\mathcal{F}_1}$, the fourth and fifth terms satisfy

$$\lambda\left\|\operatorname{div}\hat{\Psi}_u\right\|^2_{L^2(\Omega)}+\kappa|||\operatorname{div}\Psi_J|||^2_{\hat{\mathcal{I}}_\phi^{-1}}\le\frac{\lambda}{\alpha}|||\Psi_u|||^2_{\mathcal{F}_1}+\kappa(1+C_p^2)|||\Psi_J|||^2_{\mathcal{D}_J}.$$

By the definition of $\mathcal{F}_1$, we find that

$$\begin{aligned}\left|\left|\left|\mathcal{K}^*\hat{\Psi}_J\right|\right|\right|^2_{\mathcal{F}_1^{-1}}&\le\|\boldsymbol{B}_n\|_{\boldsymbol{L}^\infty(\Omega)}\left\|\hat{\Psi}_J\right\|_{\boldsymbol{L}^2(\Omega)}\left\|\mathcal{F}_1^{-1}(\mathcal{K}^*\hat{\Psi}_J)\right\|_{\boldsymbol{L}^2(\Omega)}\\&\le C_pR_e^{1/2}\|\boldsymbol{B}_n\|_{\boldsymbol{L}^\infty(\Omega)}\left\|\hat{\Psi}_J\right\|_{\boldsymbol{L}^2(\Omega)}\left|\left|\left|\mathcal{K}^*\hat{\Psi}_J\right|\right|\right|_{\mathcal{F}_1^{-1}}.\end{aligned}$$

This yields

$$\frac{\kappa^2}{\lambda}\left|\left|\left|\mathcal{K}^*\hat{\Psi}_J\right|\right|\right|^2_{\mathcal{F}_1^{-1}}\le\frac{\kappa^2C_p^2R_e}{\lambda}\|\boldsymbol{B}_n\|^2_{\boldsymbol{L}^\infty(\Omega)}\left\|\hat{\Psi}_J\right\|^2_{\boldsymbol{L}^2(\Omega)}\le\frac{\kappa}{12}\left(|||\Psi_J|||^2_{\mathcal{D}_J}+\|\Psi_\phi\|^2_{L^2(\Omega)}\right).$$

Finally, substituting the above estimates into (B.8) and using (B.6), we get

$$|||\Phi|||^2_{\mathcal{H}_0}\le(2+C_p^2)|||\Psi|||^2_{\mathcal{H}_0}.$$

The proof is completed upon using (B.2). ∎

Appendix C. The proof of Theorem 3.3.

Proof. Write $\lambda_1 = 4C_p^2\lambda$ for convenience. Direct calculations show that

$$\mathcal{P} = \begin{pmatrix} \kappa^{-1}\mathcal{D}_J^{-1} & 2\kappa^{-1}\mathcal{D}_J^{-1}\nabla & -2\mathcal{D}_J^{-1}\mathcal{K}\mathcal{F}_\kappa^{-1} & -2\mathcal{D}_J^{-1}\mathcal{K}\mathcal{F}_\kappa^{-1}\nabla\mathcal{L}_p \\ 0 & -\kappa^{-1}\mathcal{I}_\phi & 0 & 0 \\ 0 & 0 & \mathcal{F}_\kappa^{-1} & \mathcal{F}_\kappa^{-1}\nabla\mathcal{L}_p \\ 0 & 0 & 0 & -\mathcal{L}_p \end{pmatrix},$$

$$\hat{\mathcal{A}}\mathcal{P}\hat{\mathcal{H}} = \begin{pmatrix} \kappa\lambda_1\mathcal{D}_J & \kappa\lambda\nabla(\mathcal{I}_\phi - \hat{\mathcal{I}}_\phi) & -\kappa\mathcal{D}_J^{-1}\mathcal{K}\mathcal{F}_\kappa^{-1}\mathcal{F}_1 & -\kappa\mathcal{D}_J^{-1}\mathcal{K}\mathcal{F}_\kappa^{-1}\nabla \\ 0 & \kappa\lambda\hat{\mathcal{I}}_\phi & \kappa\operatorname{div}\mathcal{D}_J^{-1}\mathcal{K}\mathcal{F}_\kappa^{-1}\mathcal{F}_1 & \kappa\operatorname{div}\mathcal{D}_J^{-1}\mathcal{K}\mathcal{F}_\kappa^{-1}\nabla \\ 0 & 0 & \mathcal{F}_1 & 0 \\ 0 & 0 & 0 & -\operatorname{div}\mathcal{F}_\kappa^{-1}\nabla \end{pmatrix}.$$

For any $\xi \in \boldsymbol{X}'$, write $\Psi = \hat{\mathcal{H}}^{-1}\xi$, $\Theta = \hat{\mathcal{A}}\mathcal{P}\xi = \hat{\mathcal{A}}\mathcal{P}\hat{\mathcal{H}}\Psi$, and $\Phi = \hat{\mathcal{H}}^{-1}\Theta$. It is easy to see that

$$(\xi, \hat{\mathcal{A}}\mathcal{P}\xi)_{\hat{\mathcal{H}}^{-1}} = \langle\Psi, \Theta\rangle, \qquad |||\xi|||^2_{\hat{\mathcal{H}}^{-1}} = |||\Psi|||^2_{\hat{\mathcal{H}}}, \qquad \left|\!\left|\!\left|\hat{\mathcal{A}}\mathcal{P}\xi\right|\!\right|\!\right|^2_{\hat{\mathcal{H}}^{-1}} = \langle\Phi, \Theta\rangle. \tag{C.1}$$

Using notation similar to (B.3), we have

$$\begin{aligned} &\Theta_J = \kappa\lambda_1\mathcal{D}_J\Psi_J + \kappa(\lambda\nabla\hat{\Psi}_\phi - \hat{\Psi}_J), && \Theta_u = \mathcal{F}_1\Psi_u, \\ &\Theta_\phi = \kappa\lambda\hat{\mathcal{I}}_\phi\Psi_\phi + \kappa\operatorname{div}\hat{\Psi}_J, && \Theta_p = -\operatorname{div}\mathcal{F}_\kappa^{-1}(\nabla\Psi_p), \end{aligned} \tag{C.2}$$

where $\hat{\Psi}_J = \mathcal{D}_J^{-1}\mathcal{K}\mathcal{F}_\kappa^{-1}(\mathcal{F}_1\Psi_u + \nabla\Psi_p)$ and $\hat{\Psi}_\phi = \Psi_\phi - \hat{\mathcal{I}}_\phi\Psi_\phi$.

By Lemma A.4, $\left|\!\left|\!\left|\mathcal{F}_\kappa^{-1}(\nabla\Psi_p)\right|\!\right|\!\right|^2_{\mathcal{F}_1} = -\left(\operatorname{div}\mathcal{F}_\kappa^{-1}(\nabla\Psi_p), \Psi_p\right) \le \frac{3}{2}|||\Psi_p|||^2_{\mathcal{L}_p^{-1}}$. By arguments similar to (B.5) and using Lemma A.3, we find that

$$\begin{aligned} \left|\!\left|\!\left|\hat{\Psi}_J\right|\!\right|\!\right|_{\mathcal{D}_J} &\le \sqrt{R_eC_p^2}\,\|\boldsymbol{B}_n\|_{\boldsymbol{L}^\infty(\Omega)}\left(\left|\!\left|\!\left|\mathcal{F}_\kappa^{-1}\mathcal{F}_1\Psi_u\right|\!\right|\!\right|_{\mathcal{F}_1} + \left|\!\left|\!\left|\mathcal{F}_\kappa^{-1}(\nabla\Psi_p)\right|\!\right|\!\right|_{\mathcal{F}_1}\right) \\ &\le \sqrt{3R_eC_p^2/2}\,\|\boldsymbol{B}_n\|_{\boldsymbol{L}^\infty(\Omega)}\left(|||\Psi_u|||_{\mathcal{F}_1} + |||\Psi_p|||_{\mathcal{L}_p^{-1}}\right). \end{aligned} \tag{C.3}$$

The estimate for $\hat{\Psi}_\phi$ follows directly from Lemma A.1,

$$\left\|\hat{\Psi}_\phi\right\|_{L^2(\Omega)} \le \|\Psi_\phi\|_{L^2(\Omega)} \le (1 + C_p^2)\left\|\hat{\mathcal{I}}_\phi\Psi_\phi\right\|_{L^2(\Omega)}. \tag{C.4}$$

Using (C.2), Lemma A.4, and the assumptions of the theorem, we have

$$\begin{aligned} |||\Theta_p|||^2_{\mathcal{L}_p} &= \langle\mathcal{L}_p^{-1}\Psi_p, \Psi_p\rangle + \langle(\operatorname{div}\mathcal{F}_\kappa^{-1}\nabla - \mathcal{L}_p^{-1})\Psi_p, \mathcal{L}_p(\mathcal{L}_p^{-1} + \operatorname{div}\mathcal{F}_\kappa^{-1}\nabla)\Psi_p\rangle \\ &\le 2\,|||\Psi_p|||^2_{\mathcal{L}_p^{-1}}. \end{aligned} \tag{C.5}$$

Using (C.3)–(C.4) and Lemma A.4, we find that

$$\begin{aligned} \langle\Psi, \Theta\rangle &= \kappa\lambda_1\,|||\Psi_J|||^2_{\mathcal{D}_J} + \kappa\lambda\,|||\Psi_\phi|||^2_{\hat{\mathcal{I}}_\phi} + |||\Psi_u|||^2_{\mathcal{F}_1} - \left\langle\Psi_p, (\operatorname{div}\mathcal{F}_\kappa^{-1}\nabla)\Psi_p\right\rangle \\ &\quad -\kappa\lambda(\operatorname{div}\Psi_J, \hat{\Psi}_\phi) - \kappa(\hat{\Psi}_J, \Psi_J + \nabla\Psi_\phi) \\ &\ge \frac{3\kappa\lambda_1}{4}\,|||\Psi_J|||^2_{\mathcal{D}_J} + \frac{\kappa\lambda}{2(1+C_p^2)}\,\|\Psi_\phi\|^2_{L^2(\Omega)} + |||\Psi_u|||^2_{\mathcal{F}_1} + \frac{1}{2}\,|||\Psi_p|||^2_{\mathcal{L}_p^{-1}} \\ &\quad -\left(\frac{\kappa\lambda}{16(1+C_p^2)}\right)^{1/2}\left(|||\Psi_u|||_{\mathcal{F}_1} + |||\Psi_p|||_{\mathcal{L}_p^{-1}}\right)\left(\|\Psi_J\|_{\boldsymbol{L}^2(\Omega)} + \|\Psi_\phi\|_{L^2(\Omega)}\right) \\ &\ge \frac{1}{4(1+C_p^2)}\,|||\Psi|||^2_{\hat{\mathcal{H}}}. \end{aligned}$$

Similarly, the upper bound for $\langle \Phi, \Theta \rangle$ can be estimated as follows:

$$\begin{aligned}
\langle \Phi, \Theta \rangle &= \kappa\lambda_1 \left|\!\left|\!\left| \Psi_J \right|\!\right|\!\right|_{\mathcal{D}_J}^2 + \kappa\lambda \left\| \hat{\mathcal{I}}_\phi \Psi_\phi \right\|_{L^2(\Omega)}^2 + \left|\!\left|\!\left| \Psi_u \right|\!\right|\!\right|_{\mathcal{F}_1}^2 + \left|\!\left|\!\left| \Theta_p \right|\!\right|\!\right|_{\mathcal{L}_p}^2 + \frac{\kappa}{\lambda} \left\| \operatorname{div} \hat{\Psi}_J \right\|_{L^2(\Omega)}^2 \\
&\quad + \frac{\kappa}{\lambda_1} \left|\!\left|\!\left| \lambda \nabla \hat{\Psi}_\phi - \hat{\Psi}_J \right|\!\right|\!\right|_{\mathcal{D}_J^{-1}}^2 + 2\kappa(\Psi_J, \lambda \nabla \hat{\Psi}_\phi - \hat{\Psi}_J) + 2\kappa(\operatorname{div} \hat{\Psi}_J, \hat{\mathcal{I}}_\phi \Psi_\phi) \\
&\le 2\kappa\lambda_1 \left|\!\left|\!\left| \Psi_J \right|\!\right|\!\right|_{\mathcal{D}_J}^2 + 2\kappa\lambda \left\| \Psi_\phi \right\|_{L^2(\Omega)}^2 + \left|\!\left|\!\left| \Psi_u \right|\!\right|\!\right|_{\mathcal{F}_1}^2 + 2 \left|\!\left|\!\left| \Psi_p \right|\!\right|\!\right|_{\mathcal{L}_p^{-1}}^2 + \frac{2\kappa}{\lambda} \left\| \operatorname{div} \hat{\Psi}_J \right\|_{L^2(\Omega)}^2 \\
&\quad + \frac{2\kappa}{\lambda_1} \left|\!\left|\!\left| \lambda \nabla \hat{\Psi}_\phi - \hat{\Psi}_J \right|\!\right|\!\right|_{\mathcal{D}_J^{-1}}^2 \\
&\le 2\kappa\lambda_1 \left|\!\left|\!\left| \Psi_J \right|\!\right|\!\right|_{\mathcal{D}_J}^2 + 3\kappa\lambda \left\| \Psi_\phi \right\|_{L^2(\Omega)}^2 + 2 \left|\!\left|\!\left| \Psi_u \right|\!\right|\!\right|_{\mathcal{F}_1}^2 + 3 \left|\!\left|\!\left| \Psi_p \right|\!\right|\!\right|_{\mathcal{L}_p^{-1}}^2 \\
&\le 3 \left|\!\left|\!\left| \Psi \right|\!\right|\!\right|_{\hat{\mathcal{H}}}^2 .
\end{aligned}$$

By virtue of (C.1), the two constants can be set to $\hat{C}_{\inf} = 1/(4 + 4C_p^2)$ and $\hat{C}_{\sup} = 3$. ∎

Acknowledgment. The authors are very grateful to the anonymous referees for their constructive comments which improved the paper.

REFERENCES

[1] M. A. Abdou et al., *On the exploration of innovative concepts for fusion chamber technology*, Fusion Eng. Des., 54 (2001), pp. 181–247.

[2] S. Badia, A. F. Martín, and R. Planas, *Block recursive LU preconditioners for the thermally coupled incompressible inductionless MHD problem*, J. Comput. Phys., 274 (2014), pp. 562–591.

[3] M. Benzi, G. H. Golub, and J. Liesen, *Numerical solution of saddle point problems*, Acta Numer., 14 (2005), pp. 1–137.

[4] M. Benzi and M. A. Olshankii, *An augmented Lagrangian-based approach to the Oseen problem*, SIAM J. Sci. Comput., 28 (2006), pp. 2095–2113, https://doi.org/10.1137/050646421.

[5] D. Boffi, *Three-dimensional finite element methods for the Stokes problem*, SIAM J. Numer. Anal., 34 (1997), pp. 664–670, https://doi.org/10.1137/S0036142994270193.

[6] D. Boffi, F. Brezzi, and M. Fortin, *Mixed Finite Element Methods and Applications*, Springer-Verlag, Berlin, 2013.

[7] E. C. Cyr, J. N. Shadid, R. S. Tuminaro, R. P. Pawlowski, and L. Chacón, *A new approximate block factorization preconditioner for two-dimensional incompressible (reduced) resistive MHD*, SIAM J. Sci. Comput., 35 (2013), pp. B701–B730, https://doi.org/10.1137/12088879X.

[8] H. Dallmann, D. Arndt, and G. Lube, *Local projection stabilization for the Oseen problem*, IMA J. Numer. Anal., 36 (2015), pp. 796–823.

[9] H. Elman, V. E. Howle, J. Shadid, R. Shuttleworth, and R. Tuminaro, *Block preconditioners based on approximate commutators*, SIAM J. Sci. Comput., 27 (2006), pp. 1651–1668, https://doi.org/10.1137/040608817.

[10] J. de Frutos, B. Garcia-Archílla, V. John, and J. Novo, *Grad-div stabilization for the evolutionary Oseen problem with inf-sup stable finite elements*, J. Sci. Comput., 66 (2016), pp. 991–1024.

[11] J. F. Gerbeau, C. Le Bris, and T. Leliévre, *Mathematical Methods for the Magnetohydrodynamics of Liquid Metals*, Oxford University Press, Oxford, UK, 2006.

[12] G. Chen, D. Li, D. Schötzau, and X. Wei, *A mixed finite element method with exactly divergence-free velocities for incompressible magnetohydrodynamics*, Comput. Methods Appl. Mech. Engrg., 199 (2010), pp. 2840–2855.

[13] V. Girault and P.-A. Raviart, *Finite Element Methods for Navier-Stokes Equations*, Springer-Verlag, Berlin, 1986.

[14] T. Heister and G. Rapin, *Efficient augmented Lagrangian-type preconditioning for the Oseen problem using grad-div stabilization*, Internat. J. Numer. Methods Fluids, 71 (2013), pp. 118–134.

[15] V. E. Henson and U.M. Yang, *BoomerAMG: A parallel algebraic multigrid solver and preconditioner*, Appl. Numer Math., 41 (2002), pp. 155–177.
[16] R. Hiptmair, *Operator preconditioning*, Comput. Math. Appl., 52 (2006), pp. 699–706.
[17] R. Hiptmair and J. Xu, *Nodal auxiliary space preconditioning in* H(curl) *and* H(div) *spaces*, SIAM J. Numer. Anal., 45 (2007), pp. 2483–2509, https://doi.org/10.1137/060660588.
[18] R. Hiptmair, L. Li, S. Mao, and W. Zheng, *A fully divergence-free finite element method for magnetohydrodynamic equations*, Math. Models Methods Appl. Sci. (M3AS), 28 (2018), pp. 659–695.
[19] E. W. Jenkins, V. John, A. Linke, and G. L. Rebholz, *On the parameter choice in grad-div stabilization for the Stokes equations*, Adv. Comput. Math., 40 (2014), pp. 491–516.
[20] L. Li, M. Ni, and W. Zheng, *A charge-conservative finite element method for inductionless MHD equations. Part* I: *Convergence*, SIAM J. Sci. Comput., 41 (2019), pp. B796–B815, https://doi.org/10.1137/17M1160768.
[21] L. Li and W. Zheng, *A robust solver for the finite element approximation of stationary incompressible MHD equations in* 3*D*, J. Comput. Phys., 351 (2017), pp. 254–270.
[22] D. Loghin and A. Wathen, *Analysis of preconditioners for saddle-point problems*, SIAM J. Sci. Comput., 25 (2004), pp. 2029–2049, https://doi.org/10.1137/S1064827502418203.
[23] Y. Ma, K. Hu, X. Hu, and J. Xu, *Robust preconditioners for incompressible MHD models*, J. Comput. Phys., 316 (2016), pp. 721–746.
[24] K.-A. Mardal and R. Winther, *Preconditioning discretizations of systems of partial differential equations*, Numer. Linear Algebra Appl., 18 (2011), pp. 1–40.
[25] R. Moreau, *Magnetohydrodynamics*, Kluwer Academic Publishers, Dordrecht, the Netherlands, 1990.
[26] *MUMPS: A Parallel Sparse Direct Solver*, http://mumps.enseeiht.fr, version 5.2.1, 2019.
[27] M.-J. Ni, R. Munipalli, P. Huang, N. B. Morley, and M. A. Abdou, *A current density conservative scheme for incompressible MHD flows at a low magnetic Reynolds number. Part* I. *On a rectangular collocated grid system*, J. Comput. Phys., 227 (2007), pp. 174–204.
[28] M.-J. Ni, R. Munipalli, P. Huang, N. B. Morley, and M. A. Abdou, *A current density conservative scheme for incompressible MHD flows at a low magnetic Reynolds number, Part* II: *On an arbitrary collocated mesh*, J. Comput. Phys., 227 (2007), pp. 205–228.
[29] M. A. Olshanskii, *A low order Galerkin finite element method for the Navier-Stokes equations of steady incompressible flow: A stabilization issue and iterative methods*, Comput. Methods Appl. Mech. Engrg., 191 (2002), pp. 5515–5536.
[30] M. A. Olshanskii and A. Reusken, *Grad-div stabilization for stokes equations*, Math. Comp., 73 (2004), pp. 1699–1718.
[31] M. A. Olshanskii, G. Lube, T. Heister, and J. Löwe, *Grad-div stabilization and subgrid pressure models for the incompressible Navier-Stokes equations*, Comput. Methods Appl. Mech. Engrg., 198 (2009), pp. 3957–3988.
[32] S. Ovtchinnikov, F. Dobrain, X. Cai, and D. Keyes, *Additive Schwarz-based fully coupled implicit methods for resistive hall magnetohydrodynamic problems*, J. Comput. Phys., 225 (2007), pp. 1919–1936.
[33] E. G. Phillips, H. C. Elman, E. C. Cyr, J. N. Shadid, and R. P. Pawlowski, *A block preconditioner for an exact penalty formulation for stationary MHD*, SIAM J. Sci. Comput., 36 (2014), pp. B930–B951, https://doi.org/10.1137/140955082.
[34] E. G. Phillips, J. N. Shadid, E. C. Cyr, H. C. Elman, and R. P. Pawlowski, *Block preconditioners for stable mixed nodal and edge finite element representations of incompressible resistive MHD*, SIAM J. Sci. Comput., 38 (2016), pp. B1009–B1031, https://doi.org/10.1137/16M1074084.
[35] J. Shadid, E. Cyr, R. Pawlowski, R. Tuminaro, L. Chacón, and P. Lin, *Initial performance of fully-coupled AMG and approximate block factorization preconditioners for solution of implicit FE resistive MHD*, in Proceedings of the Fifth European Conference on Computational Fluid Dynamics (ECCOMAS CFD 2010), Lisbon, J. C. F. Pereira, A. Sequeira, and J. M. C. Pereira, eds., 2010, 1874.
[36] J. Shadid, R. Pawlowski, J. Banks, L. Chacón, P. Lin, and R. Tuminaro, *Towards a scalable fully-implicit fully-coupled resistive MHD formulation with stabilized FE methods*, J. Comput. Phys., 229 (2010), pp. 7649–7671.
[37] L. Shen and J. Xu, *On a Schur complement operator arisen from Navier-Stokes equations and its preconditioning*, in Advances in Computational Mathematics (Guangzhou, 1997), Lecture Notes in Pure and Appl. Math. 202, Z. Chen, Y. Li, C. A. Micchelli, and Y. Xu, eds., Dekker, New York, 1999, pp. 481–490.
[38] D. Schötzau, *Mixed finite element methods for stationary incompressible magneto-*

hydrodynamics, Numer. Math., 96 (2004), pp. 771–800.

[39] M. Wathen, C. Greif, and D. Schötzau, *Preconditioners for mixed finite element discretizations of incompressible MHD equations*, SIAM J. Sci. Comput., 39 (2017), pp. A2293–A3013, https://doi.org/10.1137/16M1098991.

[40] L. Zhang, *A parallel algorithm for adaptive local refinement of tetrahedral meshes using bisection*, Numer. Math. Theory Method Appl., 2 (2009) pp. 65–89. Version 0.9.2 available at http://lsec.cc.ac.cn/phg.